



# Use of industrial wastes for stabilizing expansive clays in pavement applications: durability and microlevel investigation

Z. Zimar<sup>1</sup> · D. Robert<sup>1</sup> · F. Giustozzi<sup>1</sup> · A. Zhou<sup>1</sup> · S. Setunge<sup>1</sup> · J. Kodikara<sup>2</sup>

Received: 10 April 2023 / Accepted: 13 February 2024  
© The Author(s) 2024

## Abstract

Expansive clays feature high compressibility and large swelling-shrinkage potential, which may cause significant damage to the infrastructures, including pavements. This study investigates the potential use of industrial waste ash generated from municipal solid waste incineration (MSWI) as a more sustainable treatment method to treat expansive soils compared to the use of conventional coal fly ash. A series of tests was conducted to study the mechanical, durability, and environmental performance of the MSWI fly ash in comparison with the coal fly ash. The study reveals that the compressive strength and resilient modulus of 20% MSWI fly ash treated sample increased to 0.86 MPa and 213 MPa respectively, depicting an increase of 150% and 240% of the control clay specimen. Results also indicate that MSWI treated expansive clay shows better performance during the soaked California bearing ratio (CBR) testings, moisture susceptibility and cyclic wetting–drying tests compared to coal fly ash treated samples. Microlevel investigations reveal that the influence of cation exchange is more decisive in the MSWI-treated clays due to the presence of higher  $\text{Ca}^{2+}$  ions, during the early stages, and the influence of hydration is stronger at the later stage of stabilisation. X-ray diffraction (XRD) results show that gismondine, albite, calcite, portlandite, andradite, and ettringite are the main crystalline phases formed during the stabilization. Heavy metal concentrations after the stabilisation are within the allowable limit defined by state regulations. Applying MSWI fly ash as a ground treatment for expansive clays can reduce the consumption of natural resources, promoting a “zero landfill” policy.

**Keywords** Durability · Expansive clay · MSWI fly ash · Pavement

## 1 Introduction

When experiencing recurring drying–wetting cycles, expansive clays may exhibit distinct shrinkage–swelling deformation, which causes subsidence-related cracks and heaves in houses, pavements, and buried utilities. Infrastructures built on various expansive clays are damaged, and the annual cost to repair the damage is estimated to be US \$15 billion [55]. The presence of montmorillonite, and other expansive clay minerals is the main reason for the swelling potential of these problematic clay types. These

swelling soils are found in Australia, South Africa, the UK, India, and the United States, where the groundwater level fluctuation is high during seasonal changes [48, 60]. In these circumstances, expansive clays experience unexpected climatic loadings, which degrade the hydromechanical properties of the soils. These climatic changes include sea level rise, temperature changes, flooding, wet-dry cycles, freeze–thaw cycles, and extreme rainfall. Many studies indicated that the unconfined compressive strength (UCS), shear strength, infiltration capacity, and permeability of the clays weakened drastically because of wetting and drying cycles [6, 23, 45].

These problematic soils are treated using various methods such as mechanical stabilisation, chemical treatment, and geosynthetics. Calcium-based stabilisers are commonly utilised for stabilising subgrades and bases during pavement construction. They can change the characteristics of expansive clays through the processes of

---

✉ D. Robert  
dilan.robert@rmit.edu.au

<sup>1</sup> Civil Engineering Department, School of Engineering, RMIT University, Melbourne, VIC 3001, Australia

<sup>2</sup> Civil Engineering Department, Monash University, Clayton, VIC, Australia

agglomeration, flocculation, and hydration reaction [26, 94]. Transportation agencies worldwide adopt cement, lime and fly ash for the expansive clay treatment due to the availability of well-established guidelines [44, 51]. Meanwhile, geosynthetics are proven to provide long-term durability after treatment. However, considering the budget limitations, road agencies are reluctant to choose these methods and explore cheaper industrial by-products to be used as a pavement material. Many by-products such as fly ash [81, 90, 101], slag [30, 36, 92], rice husk ash [21] and construction and demolition waste [53, 54, 79] are used to treat subgrade and base layers of the pavements. They have been proved as a good construction material for the pavement and utilized by geotechnical engineers to enhance the stiffness of the expansive clay while reducing the potential for more waste to landfills.

Coal fly ash is a comparatively cheap cementitious material produced from coal power plants and categorized as class C and F fly ash. UCS, CBR and resilient modulus ( $M_r$ ) increased with the fly ash addition and curing period for most clay soils except peat [46, 58, 83, 101]. Pozzolanic reaction and flocculation increase the strength and reduce the swelling potential of the fly ash stabilised samples [18, 66]. Class C fly ash performs well due to its self-cementitious nature compared to the type F fly ash in the stabilisation [101]. However, class C fly ash is not widely available in many countries, including Australia, India, Japan, China and some other European countries [15, 17, 43]. There are limited studies conducted on the mechanical [71, 98] and hydraulic performance of class F fly ash stabilised [20, 25] expansive clays. An in-depth study, however, has not been conducted on the reaction mechanism and durability of class F fly ash stabilised high plasticity clays. Municipal solid waste incineration fly ash (MSWI fly ash), which is produced by burning solid wastes at the waste to energy (WTE) plants, is now becoming a topic of focus among practitioners and researchers.

Solid waste production is predicted to rise to 2.2 billion tons per day worldwide by 2025 [47]. The incineration of solid waste is one of the most common ways of managing solid waste globally [82]. This incineration process reduces large landfilling waste volume and produces energy in the form of heat or electricity. More than 2000 incineration plants are established worldwide [64], burning several million tons of solid waste annually. In Western Europe alone, 1.2 million tons of MSWI fly ash is produced yearly [39]. MSWI fly ash is considered hazardous waste and landfilling this waste can cause many environmental issues as it contains a significant amount of heavy metals such as Ni, Cd, Pb, As, Hg and As [68, 78]. Cement solidification, chemical stabilisation and thermal separation are some of the treatment methods to reduce the heavy metal

concentration from MSWI fly ash [97]. During stabilisation, several crystalline cementation bonds form and encapsulate the heavy metals while providing good structural performance. There are few studies available on the MSWI fly ash usage for pavement stabilisation and ground improvement [75, 87, 91, 93, 100], and they primarily focused on the mechanical performance, swelling-shrinkage potential and leaching potential. Expansive clay experienced negligible settlement (0.04 mm) after stabilisation with 15% MSWI fly ash. Further, 20% MSWI fly ash treated samples showed 46% less shrinkage than the control sample [100]. Many studies have concluded that the leaching of MSWI fly ash treated pavements are within the acceptable limit [57, 87, 91]. However, the long-term durability along with the relevant microstructural investigation and the pavement stability under repeated stress have not been paid enough attention in past research.

The design guidelines for the stabilization of expansive clay recommend the least possible percentage of additives to achieve the minimum required strength. However, several transportation agencies claimed premature failures in the stabilised pavement due to seasonal changes and loss of stabilizers [24]. Therefore, the stabiliser's long-term behaviour and seasonal performance need to be investigated to understand the interaction between the chemical additive and clay minerals. Stabilised subgrades are unavoidably exposed to cyclic climate loadings such as drying-wetting, flooding, freezing-thawing and temperature variations which significantly influence the durability of pavements. Stabilised subgrades subjected to varying climatic conditions can degrade the long-term hydro-mechanical performance of compacted subgrades. Therefore, the durability of the stabilised soils needs to be assessed during the design stage to understand the climatic impact.

Most pavement stabilisation studies primarily focus on strength variation and mass loss after a number of weathering cycles. However, these macro-scale lab testings do not explain the degradation mechanism associated with climatic changes. The chemical and mineralogical changes in the interparticle bonding can be well demonstrated using micro level investigation. Microstructural analyses of stabilised soil mixes help to understand the interaction between soil minerals and the binder, and support explaining the mechanical and durability characteristics. However, microlevel investigation on MSWI fly ash treated expansive clays has not been extensively studied in the past. Therefore, the present study aims to investigate the performance of MSWI fly ash in pavement geotechnics compared to class F coal fly ash. A multi-scale investigation was conducted on MSWI and class F (FFA) fly ash stabilised high plasticity clay to evaluate the mechanical, durability and leaching performance while investigating

the reaction mechanism using chemical and micro level analysis.

In this study, a series of experiments was carried out to explore the possible use of industrial wastes for stabilizing expansive clays in pavement applications. UCS test, California bearing ratio (CBR) and resilient modulus test were performed to study the mechanical characteristics. The durability was examined by conducting 4 and 10 days soaked CBR tests, moisture susceptibility and wet and drying testing, while the leaching potential was studied using the Australian bottle leaching test. In addition to the mechanical and durability testing, a series of chemical and microstructural analyses were performed on stabilised and wet-dried samples. X-Ray diffraction (XRD), thermogravimetric analyses (TGA) and fourier transform infrared spectroscopy (FTIR) have been used to understand the chemical and mineralogical change with the curing time and different wetting-drying cycles. Scanning electron microscopy (SEM) tests were performed to evaluate the microstructural changes during the MSWI/coal fly ash modification and to analyse wetting and drying effects.

## 2 Experimental procedure

### 2.1 Materials

In this study, expansive clay, MSWI fly ash and FFA were sourced in Melbourne, Australia. Particle size distribution was performed using a hydrometer and sieve for the soil, while Malvern Mastersizer 3000 was used for the size distribution of MSWI fly ash and FFA (Fig. 1). Atterberg limits testing was conducted for the expansive soil using AS 1289.3.2.1 [2] and it was found that the liquid limit and

the plasticity index are 62 and 34, respectively. Therefore, the soil was classified as CH (high plasticity clay) according to the Unified Soil Classification System. Mineralogical and chemical compositions of the raw materials were studied using X-ray fluorescence (XRF), XRD and SEM testing.

XRF and XRD testings were conducted for soil samples to determine the elements, oxides and crystalline structures present. It is clear from Table 1 that expansive soil has alumina, silica, calcium, and iron in major amounts and other elements in minor quantities. Also, it was found that  $\text{Al}_2\text{O}_3$ ,  $\text{SiO}_2$ ,  $\text{CaO}$ ,  $\text{Fe}_2\text{O}_3$ , and  $\text{Na}_2\text{O}$  are present as oxides in the clay. XRD pattern of the clay sample indicates the presence of quartz, montmorillonite, illite, and kaolinite and these minerals are responsible for the expansive nature of the clay.

SEM, XRF and XRD analyses were performed for MSWI fly ash and FFA. SEM images of MSWI fly ash and FFA are shown in Fig. 2. MSWI fly ash consists of irregular unbound carbons and hollow spheres. FFA images showed more hollow spheres compared to MSWI fly ash. XRF results (Table 1) show that Ca, Cl, Al, Si, Ti, and Fe are the major elements in the MSWI fly ash. Higher chlorine in the MSWI fly ash is due to the plastic waste in the solid wastes [62, 85]. Therefore, using MSWI fly ash in reinforced concrete can be challenging as it may lead to corrosion. XRF results also revealed that  $\text{CaO}$ ,  $\text{SiO}_2$ ,  $\text{Al}_2\text{O}_3$ ,  $\text{TiO}_2$ ,  $\text{Fe}_2\text{O}_3$ , and  $\text{MgO}$  are the major oxides present in the MSWI fly ash. Meanwhile, FFA comprises more Si, Al, Ca, and Fe elements and  $\text{SiO}_2$ ,  $\text{Al}_2\text{O}_3$ ,  $\text{Fe}_2\text{O}_3$ , and  $\text{CaO}$  as major oxides. The ratio of  $\text{CaO}/\text{SiO}_2$  and  $\text{CaO}/$

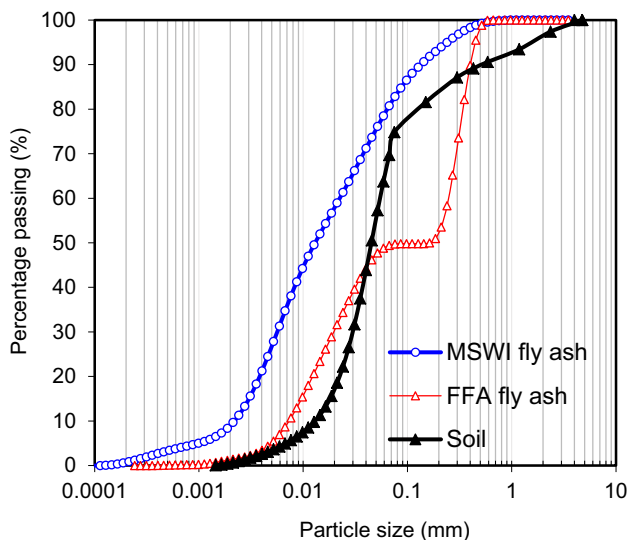


Fig. 1 Particle size distribution of soil, MSWI fly ash and FFA

Table 1 Elements and oxides in the raw materials

Element	MSWI	FFA	SOIL	Oxides	MSWI	FFA	Soil
Na	0.66	0.47	0.32	$\text{Na}_2\text{O}$	1.20	1.02	0.60
Mg	0.76	0.22	0.51	$\text{MgO}$	1.22	0.49	1.04
Al	2.30	10.06	4.01	$\text{Al}_2\text{O}_3$	4.24	22.00	8.34
Si	3.42	22.40	16.90	$\text{SiO}_2$	6.72	48.50	35.99
P	0.33	0.15	0.13	$\text{P}_2\text{O}_5$	0.62	0.30	0.26
S	0.36	0.09	0.02	$\text{SO}_3$	0.70	0.19	0.05
Cl	16.97	0.00	0.14	$\text{K}_2\text{O}$	0.30	1.60	1.00
K	0.28	1.59	0.94	$\text{CaO}$	52.60	2.83	3.71
Ca	45.77	2.56	3.10	$\text{TiO}_2$	2.27	0.96	1.12
Ti	1.63	0.77	0.80	$\text{Cr}_2\text{O}_3$	0.04	0.01	0.02
Cr	0.03	0.01	0.02	$\text{MnO}$	0.04	0.05	0.09
Mn	0.03	0.05	0.08	$\text{Fe}_2\text{O}_3$	1.25	3.10	6.06
Fe	1.19	3.02	5.12				
Cu	0.51	0.01	0.01				
Zn	0.35	0.02	0.01				
Sr	0.11	0.21	0.06				

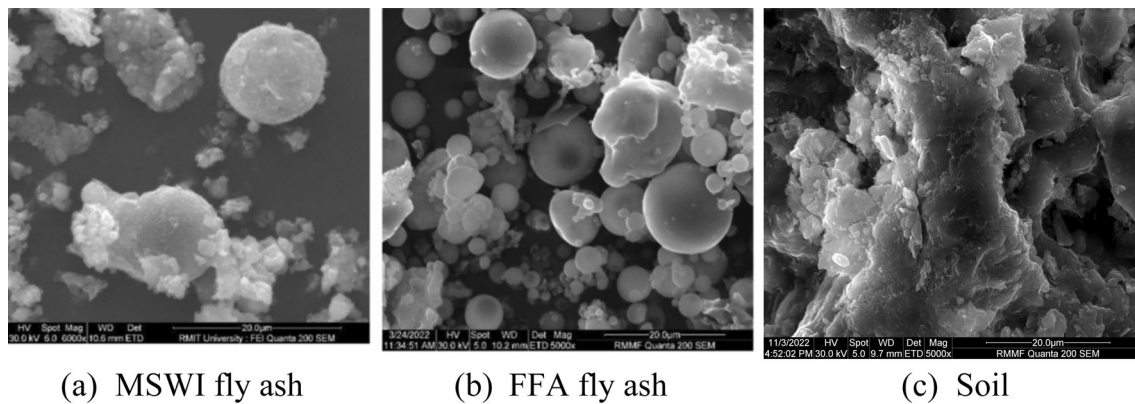


Fig. 2 SEM images of **a** MSWI fly ash, **b** FFA and **c** soil

( $\text{SiO}_2 + \text{Al}_2\text{O}_3$ ) are used as indicators to explain the potential pozzolanic reactions during the hydration process [52, 69]. MSWI fly ash has higher  $\text{CaO}/\text{SiO}_2$  and  $\text{CaO}/(\text{SiO}_2 + \text{Al}_2\text{O}_3)$  ratios of 7.8 and 4.8, while ratios of only 0.06 and 0.04, respectively, were found in FFA. Therefore, MSWI fly ash has a higher potential for excellent pozzolanic characteristics compared to the FFA. XRD diagram of the MSWI fly ash and FFA are shown in Fig. 3. Portlandite, gehlenite, calcite, and calcium chloride hydroxide are the main crystalline phases identified in the MSWI fly ash, whereas FFA consists of mullite ( $3\text{Al}_2\text{O}_3\cdot 2\text{SiO}_2$ ), silicon oxide, hematite, and calcite.

## 2.2 Sample preparation and test program

Figure 4 shows the flow chart of the test program and Table 2 summarizes the test conditions and the standards followed in this study. Fly ashes were mixed in 10%, 15%, and 20% dosages by weight of dry soil. The incorporation of fly ashes at dosages comprising 10%, 15%, and 20% by

weight of dry soil was undertaken to understand how the percentage variation of fly ash affects the soil stabilization properties. These proportions were selected as a starting point for this study to explore a reasonable range of ratios that could potentially provide adequate stabilization. Another basis for this selection evolves from the existing research works on coal fly ash which was also tested in similar range in general [18, 31, 58, 65, 98]. Many of these studies have claimed that the inclusion of coal fly ash exceeding 20% is considered ineffective for stabilization purposes, as it predominantly persists in the final product as unreacted residues. Most of the tests were conducted after 7 and 28-day air curing. CBR tests were performed after 4 and 10 days of soaking as recommended in the Austroads guidelines [12]. Following the tests for physical properties of raw materials, mechanical and durability tests were conducted for stabilised samples. Then, wet-dry and environmental testings were performed for the control soil and optimum mix (20% MSWI fly ash). Microlevel investigations (XRD, FTIR, TGA, and SEM) were conducted for all

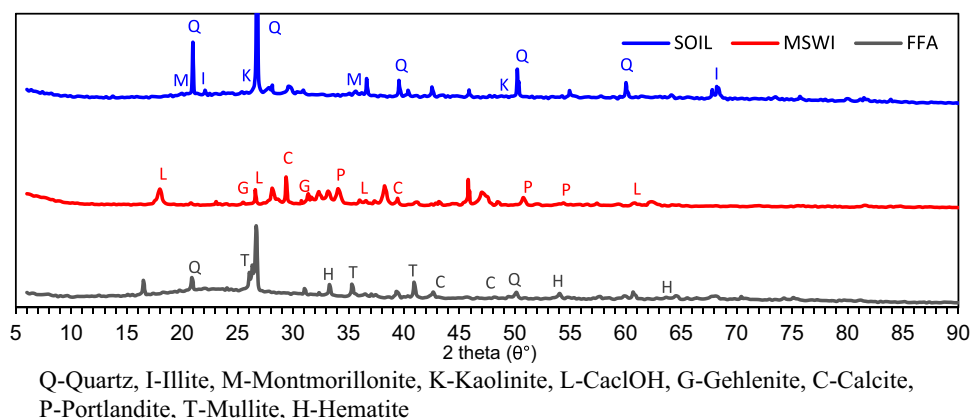


Fig. 3 XRD of the raw materials

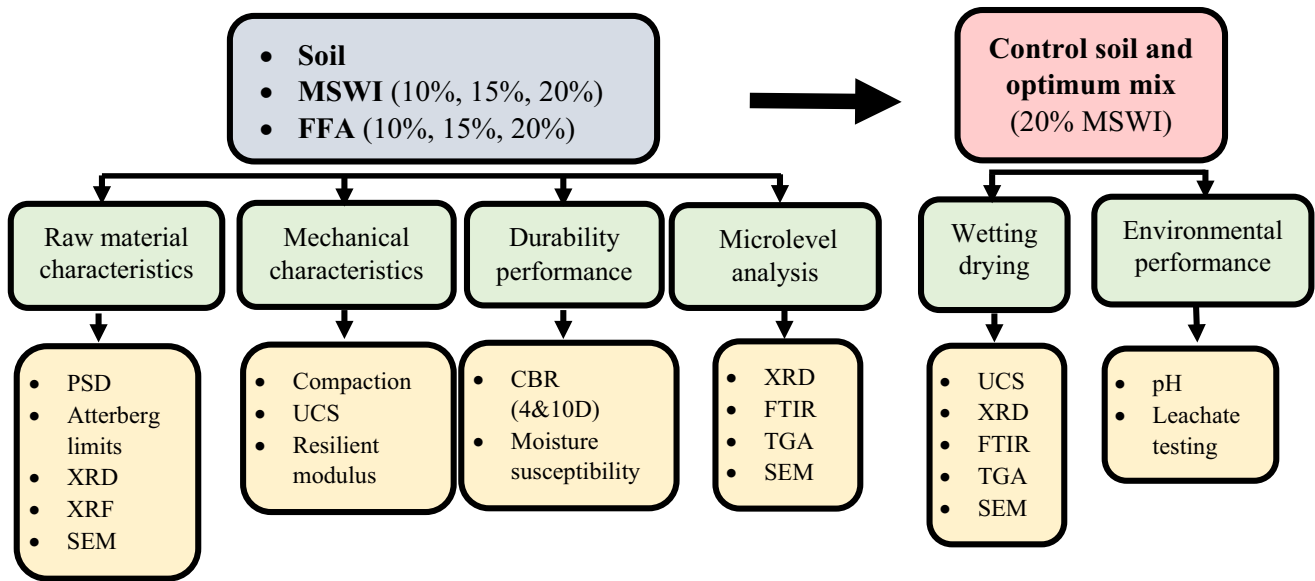


Fig. 4 Flow chart of the test program

the stabilised and weathered samples to understand the stabilisation mechanism and weathering process.

The soil was oven dried at 105 °C for 24 h and sieved through a 4.75 mm sieve. The oven-dried soil is mixed with water and cured for 4 days as recommended in AS 1289.6.1.1:2014. After 4 days of curing, cured soil was mixed with MSWI fly ash/FFA at a suitable dosage. Optimum moisture content (OMC) and the maximum dry density (MDD) were determined using the standard proctor compaction testing. All the samples for the testings were prepared at OMC + 1% and compacted within 15 min. The additional moisture is provided to support the hydration reaction of the fly ashes and to accommodate moisture loss during the soil curing process. The compaction time was maintained to a value similar to the field compaction duration using a padfoot type roller, as suggested by Ferguson and Levorson [37].

## 2.2.1 Test procedure

**2.2.1.1 Compaction test** The compaction test was performed using the standard proctor compaction energy based on AS 1289.1.1:2017 [1] to determine the optimum moisture content and maximum dry density.

**2.2.1.2 UCS test** The UCS test was conducted at a 1 mm/min deformation rate using the AS 5101.4:2008 [11]. Soil samples were mixed with OMC + 1% moisture and cured inside sealed bags for 4 days. Samples were mixed with the required percentage of additive and air cured inside the

humidity chamber at 95% humidity and 20° C. UCS testings were performed for 7 and 28-day air cured samples.

**2.2.1.3 Resilient modulus test** Resilient modulus testing was conducted in accordance with the AASHTO T307-99 [4] using reconstituted cylindrical specimens. This test is used to design pavement structures by evaluating the pavement structural response to wheel loads. Samples were prepared in the resilient modulus testing mould (100 mm diameter and 200 mm height) at OMC + 1% moisture to the MDD and tested following the loading sequence mentioned in Table 3. Initially, a preconditioning confining pressure of 41.4 kPa was applied to the specimen for 1000 loading cycles. After the conditioning phase, the maximum axial stress was reduced to 13.8 kPa, setting the confining pressure to 41.4 kPa. The test was continued for the remaining load sequences, as shown in Table 3, by applying 100 repetitive loading of the corresponding cyclic stress. The corresponding recovered deformations were recorded using Linear Variable Differential Transformers (LVDT) for each loading sequence. In all the tests, a contact stress of 10 percent of the maximum applied axial stress was maintained as recommended in AASHTO T307-99 [4]. The resilient strain ( $\epsilon_r$ ) and resilient modulus ( $M_r$ ) were calculated using Eqs. 1 and 2 respectively, for each loading sequence.

$$\epsilon_r = e_r/L \quad (1)$$

$$M_r = S_{cyclic}/\epsilon_r \quad (2)$$

**Table 2** Experimental tests

Tests	Conditions	Standards
Compaction test		AS 1289.5.1.1:2017 [1]
UCS test	7 & 28 days	AS 5101.4:2008 [11]
Resilient modulus	7 & 28 days	AASHTO T307-99 [4]
CBR (4D & 10D soaked)	4 & 10 days soaked	AS 1289.6.1.1:2014 [3]
Moisture susceptibility	7 days	AS 5101.4-2008 [11]
Wet-dry	(0WD, 1WD, 3WD, 6WD, 6WD + 24SD, 6WD + 48SD) cycles	ASTM D559/D559M-15 [8]
pH	7 & 28 days	Rayment and Lyons (2011) [80]
Leachate testing	7 & 28 days	AS 4439.3: 2019 [10]
XRD	7 & 28 days, (0WD, 1WD, 3WD, 6WD, 6WD + 24SD, 6WD + 48SD) cycles	
FTIR		
TGA		
SEM		

UCS = Unconfined compressive strength, CBR = California bearing ratio, XRD = X-ray Diffraction, FTIR = Fourier transform infrared spectroscopy, TGA = Thermogravimetric analysis, SEM = Scanning Electron Microscopy, MSWI fly ash = Municipal solid waste incineration fly ash, FFA = Class F fly ash, WD = Wet-dry cycles, 24SD = 24 h soaking and 24 h drying

where  $e_r$  is the resilient axial deformation due to  $S_{cyclic}$ ;  $S_{cyclic}$  is cyclic applied axial stress.

**2.2.1.4 CBR test** CBR test was conducted according to AS 1289.6.1.1:2014 [3]. Soil samples were mixed with water and cured for 4 days, then they were mixed with the required dosage of MSWI FA/FFA and compacted. Compacted specimens were consequently air cured for 4 days

and then soaked in water for another 4 days. CBR test was conducted for the 4 days-soaked samples at 1 mm/min penetration rate.

Ten days conditioning was conducted for soaked CBR testing to simulate and study the performance of stabilised samples during a severe rainfall event. Austroads recommends [12] 10 days of soaked CBR testing for extreme rainfall events above 800 mm, and when the drainage condition is classified as fair to poor. Thus, 10 days of soaked CBR testing was conducted for all the samples as per AS 1289.6.1.1:2014 [3]. Samples were compacted at the OMC and MDD followed by air curing for 4 days to allow for the hydration reaction. Then, specimens were soaked for 10 days before conducting CBR testing.

**Table 3** Loading sequences of resilient modulus testing

Sequence no	Confining pressure (kPa)	Maximum axial stress (kPa)	Cyclic stress (kPa)	No of load applications
0	41.4	27.6	24.8	1000
1	41.4	13.8	12.4	100
2	41.4	27.6	24.8	100
3	41.4	41.4	37.3	100
4	41.4	55.2	49.7	100
5	41.4	68.9	62	100
6	27.6	13.8	12.4	100
7	27.6	27.6	24.8	100
8	27.6	41.4	37.3	100
9	27.6	55.2	49.7	100
10	27.6	68.9	62	100
11	13.8	13.8	12.4	100
12	13.8	27.6	24.8	100
13	13.8	41.4	37.3	100
14	13.8	55.2	49.7	100
15	13.8	68.9	62	100

**2.2.1.5 Moisture susceptibility test** The moisture susceptibility test was conducted to investigate the load-carrying capacity of stabilised samples due to moisture. Tests were performed according to AS 5101.4-2008 [11], and samples were prepared similarly to the UCS testing samples. All the samples were air cured for 7 days inside the humidity chamber at 20 °C and 95% humidity. After the curing, samples were immersed in water for 4 h at a temperature of 20 °C, and then removed from the curing tank and drained for 15 min before the compression testing.

## 2.2.2 Microlevel analysis

A series of chemical and microlevel testings were conducted to understand the chemistry of the stabilisation process and to explore the micro-structural changes after the stabilisation process. Microlevel investigation was

performed on all the stabilised and wet and dried samples. XRD, TGA, FTIR, and SEM analyses were conducted on the control and stabilised samples after 7 and 28 days of curing. Also, 20MSWI fly ash treated samples were analysed after 0WD, 1WD, 3WD, 6WD and 6WD + 24SD to understand the degradation mechanism of MSWI fly ash treated clays.

**2.2.2.1 XRD test** XRD test was conducted using powder materials from the UCS testing samples to analyse the crystalline structure before and after the stabilization. Powder samples were placed in the stainless-steel holder, and the surface was smoothed and placed inside the D4 Endeavor diffractometer at 40 kV voltage and 35 mA current operating conditions. Diffraction graphs were then analysed using DIFFRAC.EVA V5.0 software.

**2.2.2.2 TGA analysis** TGA analysis was conducted to determine additives' thermal stability and to investigate their fraction of volatile components. The test is performed using 3–5 mg powdered samples with the TGA8000 Perkin Elmer in an N<sub>2</sub> atmosphere. Initially, nitrogen gas was introduced into the TGA chamber for 3 min to expel oxygen. After that, the temperature was increased from 40 °C to 850 °C at the rate of 10 °C per min. Each test took approximately 90 min, and TGA and DTG curves were obtained from the software.

**2.2.2.3 FTIR spectroscopy** FTIR spectroscopy was used to identify and characterize materials after the soil stabilisation. UCS-tested samples were crushed into fine powders using a mortar and pestle. A small amount of sample was placed into the FTIR spectrometer. The spectrometer measured the range of wavelengths in the infrared region that are absorbed by the material. FTIR spectra were obtained at the 32 scans average and in the range of 400 cm<sup>-1</sup> to 4000 cm<sup>-1</sup>.

**2.2.2.4 SEM analysis** SEM test was conducted for control and stabilised samples using the FEI Quanta 200. Powder samples obtained after UCS testing (7 and 28 days of air curing) were coated with a thin layer of iridium using a sputter coater. SEM images were obtained at the 10 mm working distance and spot size of 5 using 25 kV of energy.

## 2.2.3 Wetting and drying test

Pavement subgrades undergo significant volumetric deformations during the wetting–drying cycles. Therefore, the performance of stabilised expansive clays were assessed under cyclic drying-wetting conditions. Wet-dry testing was conducted for control and 20MSWI stabilised samples

following the ASTM D559/D559M-15 [8]. Samples were air cured for 7 days before wet-drying testing and then submerged in water for 5 h. Then, they were placed in an oven at 70 °C for 42 h. This process was considered as 1 cycle. Wet-dry tests were conducted after 1, 3, and 6 cycles. After 6 cycles, another two tests were conducted by soaking and drying the samples for a more extended period. The first sample was dried and soaked for 24h, and the other sample was soaked for 48 h and dried for 48 h. After cycling wetting–drying, UCS testing was conducted for the samples using AS 5101.4:2008 [11].

## 2.2.4 pH and leachate test

pH testing was conducted using water and 0.01M calcium chloride extract following the soil chemical methods handbook [80]. Soil samples were diluted with water in a 1:5 ratio and shaken for 1 h using a mechanical shaker.

Leachate testing was conducted following the Australian bottle leaching procedure (ABLP) AS 4439.3: 2019 [10]. After the 7 days of UCS testing, the control and 20 other MSWI fly ash treated samples were collected for the testing. Samples were crushed and sieved through a 2.4 mm sieve, and they were leached through pH 5.0 and pH 7.0 buffers. Water was used as the pH 7.0 buffer. The leaching fluid pH 5.0 was prepared by adding 5.7 ml glacial acetic acid to 900 ml of water. Then, 64.3 ml of 1 mol/L sodium hydroxide solution was added and diluted to 1 L using water. Samples were prepared on a 1:20 ratio in bottles by mixing 5 g of sample with 100 ml pH 7.0 or pH 5.0 buffer. All the bottles were then placed in an agitator and rotated for 18 h at 28 rotations per minute. The extracted fluid was filtered using a glass fibre filter to separate the solid particles. The leached solution was then analysed using the ICP-MS for heavy metals, including iron (Fe), cadmium (Cd), lead (Pb), mercury (Hg), arsenic (As), barium (Ba), nickel (Ni), titanium (Ti), chromium (Cr), copper (Cu), and zinc (Zn).

## 3 Results and discussion

### 3.1 Mechanical and durability characteristics

#### 3.1.1 Compaction

The compaction behaviour of the stabilised samples is illustrated in Fig. 5, which shows the relationship between the maximum dry density and the initial moisture content of the mixture. In general, MSWI fly ash stabilised samples show a downward shift, whereas an upward left shift can be observed for the FFA stabilised clays. The results show that the control sample's maximum dry density and optimum

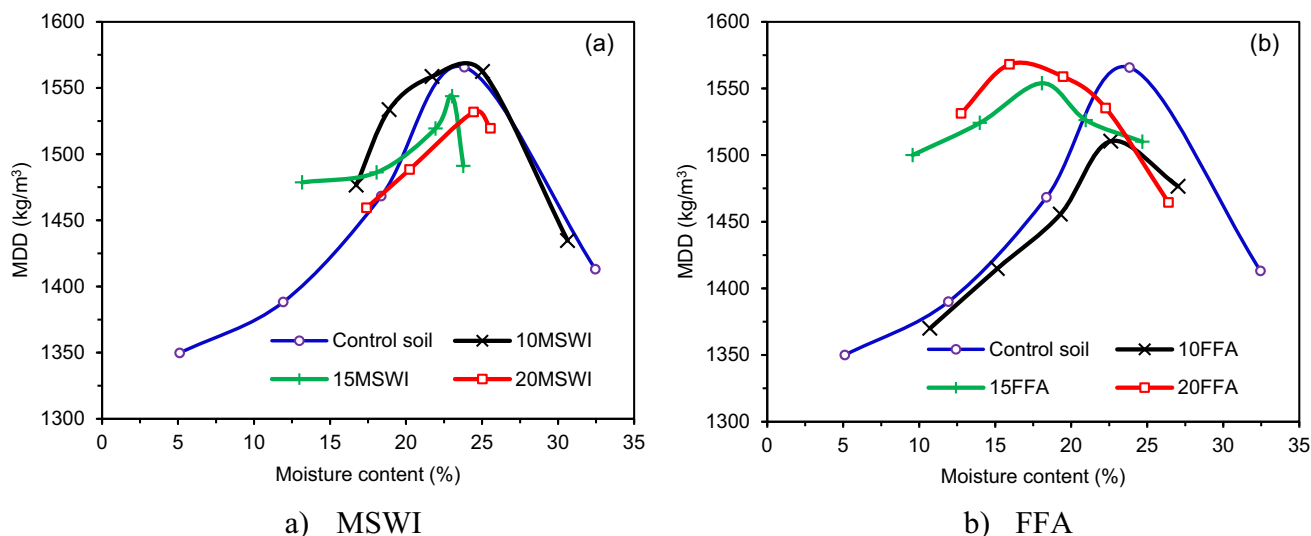


Fig. 5 Compaction characteristics of a MSWI fly ash b FFA treated clays

moisture content are 1565.7 kg/m<sup>3</sup> and 23.8%, respectively.

MDD of the MSWI fly ash stabilised samples decrease with the addition of MSWI fly ash, whereas an increasing trend for MDD is observed for the FFA. The MDD of 20% MSWI fly ash and 20% FFA treated samples are 1531.8 kg/m<sup>3</sup> and 1568 kg/m<sup>3</sup>, respectively. Hydration reactions and cation exchange are the main reasons for the density variation when a chemical additive is added to the clayey soil [18]. Hydration increases the MDD of the sample by occupying the voids in the soil. In contrast, cation exchange between Ca<sup>2+</sup> ions in the stabilizer and clay particles neutralizes the clay, and reduces the thickness of the diffuse double layer of the clay [76]. Ca<sup>2+</sup> ions are firmly held near the soil surface, and the double positive charge attracts anions of clay particles. Therefore, clay minerals agglomerate and increase the particle size and total volume, reducing the MDD. MSWI fly ash has higher calcium content, and the influence of cation exchange is stronger for the MSWI fly ash treated clay samples during the early stages of mixing. However, cation exchange reaction is not dominant in the FFA treated clays due to the lower content of CaO in the fly ash. Therefore, the hydration process is predominant in FFA stabilised clays compared to the cation exchange.

### 3.1.2 UCS

The UCS of the stabilized clay specimens after 7 and 28 days of air curing are shown in Fig. 6. The UCS of MSWI fly ash stabilised samples increase with the addition of MSWI fly ash and curing time. Compressive strength of the 10%, 15%, and 20% MSWI fly ash stabilised samples are 0.48, 0.74, and 0.86 MPa respectively, after 7 days of

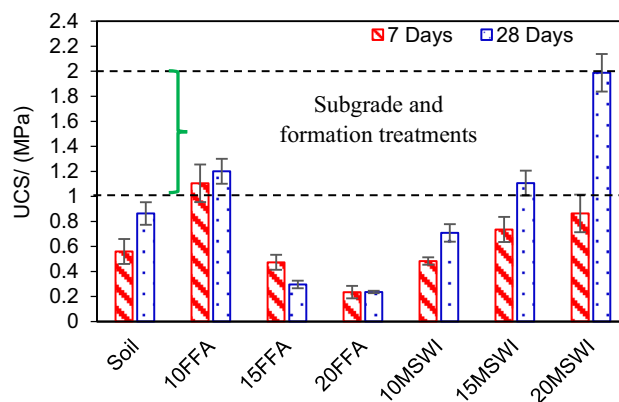


Fig. 6 UCS of stabilised samples after 7 and 28 days air curing

curing. In 28 days, the UCS increases to 0.71, 1.1, and 2 MPa for the 10MSWI, 15MSWI, and 20MSWI fly ash treated clays, respectively. Compressive strength increments of 20MSWI after 7 and 28 days are about 150% and 230% higher than the strength of control clayey soil. On the other hand, UCS of FFA stabilised clays increase after adding 10% fly ash and decrease beyond 10%. UCS of 10FFA is 1.1 MPa and 1.2 MPa after 7 and 28-days curing respectively. After 7 days of air curing, UCS of 15% and 20% FFA treated samples are 0.47 and 0.23 MPa. The compressive strengths of the 15% and 20% FFA added samples are reduced to 0.29 MPa and 0.24 MPa respectively, after 28 days of curing.

MSWI fly ash contained more than 50% CaO and greater CaO/SiO<sub>2</sub> and CaO/(SiO<sub>2</sub> + Al<sub>2</sub>O<sub>3</sub>) ratios. Therefore, MSWI fly ash can provide a stronger cationic exchange reaction and crystalline formation during the hydration process, leading to significant strength gains. MSWI fly ash, when combined with the soil, mitigates the



natural expansion and shrinkage tendencies of expansive soil. 20% MSWI fly ash treated samples experienced 46% less shrinkage than the control soil [101]. The combination of the hydration process facilitated by the fly ash and the concurrent reduction in soil shrinkage collectively enhance the mechanical performance of the treated soil. On the other hand, FFA only contains a small percentage of CaO (2.83%) and low CaO/SiO<sub>2</sub> and CaO/(SiO<sub>2</sub> + Al<sub>2</sub>O<sub>3</sub>) ratios. Therefore, FFA stabilised samples do not show a significant strength gain compared to MSWI FA. The additional FFA beyond 10% did not react during the hydration process and stayed in the mixture as unbound silt particles, hence decreased the UCS.

Austrorads [13] recommend UCS between 1 and 2 MPa for the material to be used as a stabilised subgrade material. Therefore, 10% FFA and 15–20% MSWI fly ash are found to be suitable as a subgrade stabiliser for pavements during the dry weather condition. The role of MSWI FA and FFA in the composite material is further discussed in Sect. 3.4 using results from the microstructural analysis.

The UCS results were compared with findings from lime-stabilized high-plasticity clays. Bell [14] investigated the stabilization of high-plasticity montmorillonite and kaolinite using lime, with lime additions ranging from 0 to 10% and observed that with a 4% lime addition, montmorillonite and kaolinite achieved compressive strengths of 0.8 MPa and 1 MPa, respectively. Similarly, in another study [59], lime stabilization of kaolinite clay using lime additions ranging from 0 to 12% revealed that a 4% lime addition resulted in a compressive strength of 1 MPa. Consequently, the UCS values obtained for 15–20% MSWI fly ash-treated subgrade materials are comparable to those achieved through lime stabilization, despite the use of a lower percentage of lime in the latter method.

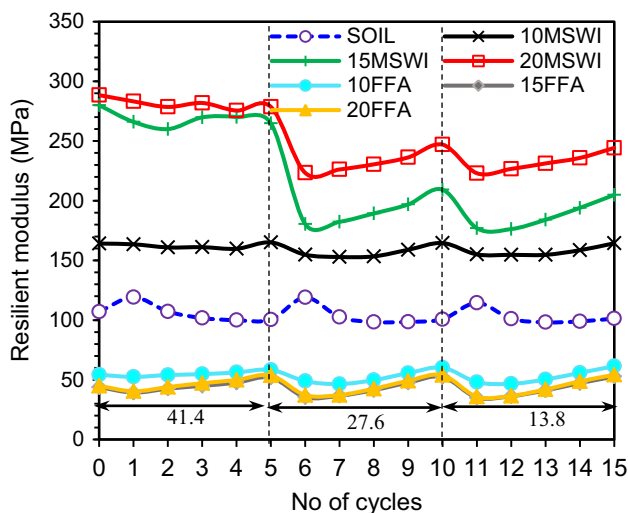


Fig. 7 Resilient modulus with different cyclic loadings

### 3.1.3 Resilient modulus

Figure 7 shows the axial  $M_r$  of the control and stabilised samples after 7 days of air curing with the loading sequences. During the resilient modulus testing, three confining stresses (41.4, 27.6, and 13.8 kPa) were maintained throughout the test.  $M_r$  generally increases with confining stress increment and decreases with the deviator stress. With the confining stress increment, soil and additive particles closely bond with each other which increases the  $M_r$ . Figure 7 shows a decrease in the  $M_r$  when the confining stress is switched from 41.4 to 27.6 kPa (6th cycle) and from 27.6 to 13.8 kPa (11th cycle). Control soil, 10MSWI and all the FFA stabilised samples do not show a significant variation with the different loading sequences. However, a considerable variation in the  $M_r$  can be observed for the 15% and 20% MSWI fly ash treated specimens.

There is a slight decrease in resilient modulus with the deviator stress increment for 1–5 cycles. During these stages, the confining stress was set to 41.4 kPa, and the deviator stress was gradually increased, as shown in Table 3. During the deviator stress increment, load-induced damage could have happened for the 15% and 20% MSWI fly ash stabilised samples as their stiffnesses are high due to the higher CaO content. This load-induced damage could have decreased the  $M_r$  value slightly. Other researchers also reported a similar trend of increasing  $M_r$  with the increment of confining stress and reduction in deviator stress for the subgrade materials [38, 72, 77]. Nevertheless, after the 5th cycle, the resilient modulus slightly increased with the deviator stress increment which is due to the particle packing occurring in the low confining stress region (27.6 kPa and 13.8 kPa).

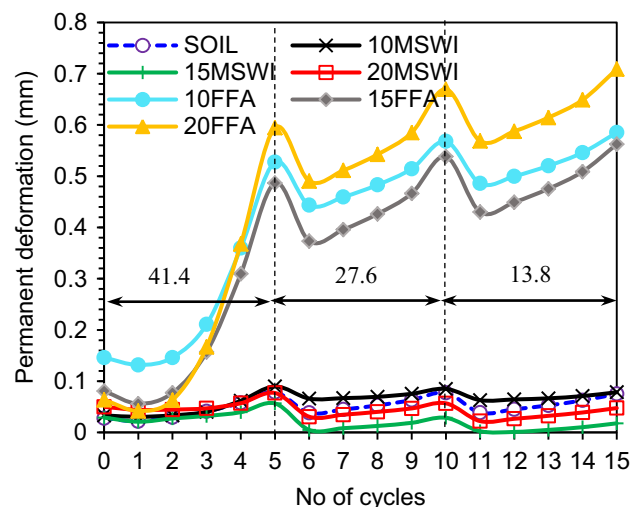


Fig. 8 Permanent deformation with different cyclic loadings

Figure 8 shows the permanent deformation of the treated samples after 7 days of curing. Overall, permanent deformation increases with the deviator stress for a constant confining pressure. Control and MSWI fly ash treated samples show less than 0.1 mm deformation in all the loading sequences. Expansive clay performs well after 7 days of air curing conditioning. During the air curing period, expansive clay loses moisture and shrinks, increasing the clay's stiffness, which ultimately increases the  $M_r$  of the clay sample. MSWI fly ash has higher pozzolanic behaviour and creates more hydration products which improves  $M_r$ . On the other hand, FFA stabilised samples exhibit a significant deformation under different loading conditions. FFA does not have higher ratios of  $\text{CaO}/\text{SiO}_2$  and  $\text{CaO}/(\text{SiO}_2 + \text{Al}_2\text{O}_3)$ . Therefore, FFA treated samples do not have greater number of strong pozzolanic hydrated products. Although, 10% FFA sample showed a significant compressive strength, it does not bear the cyclic loading, thus exhibits considerable deformation. 20% FFA added samples show a significant deformation of 0.7 mm after 15 loading cycles.

Figure 9 shows the average resilient modulus ( $M_r$ ) of stabilised clays after 7 and 28 days of curing. The resilient modulus of treated clays increased with MSWI fly ash addition. The resilient modulus of the expansive clay increased from 89 to 135, 175, and 213 MPa after adding 10%, 15%, and 20% MSWI fly ash, respectively after 7 days of curing time. Similarly, there is a significant increase in the average resilient modulus of the MSWI fly ash treated clays compared to the control sample after 28 days of curing. The resilient modulus of the 20MSWI fly ash treated sample increased about 220% of the control soil specimen in 28 days. The average modulus of the 10%, 15%, and 20% FFA treated clays are 53.3, 37, and 38.1 MPa after 7 days of curing. All these values are lower than

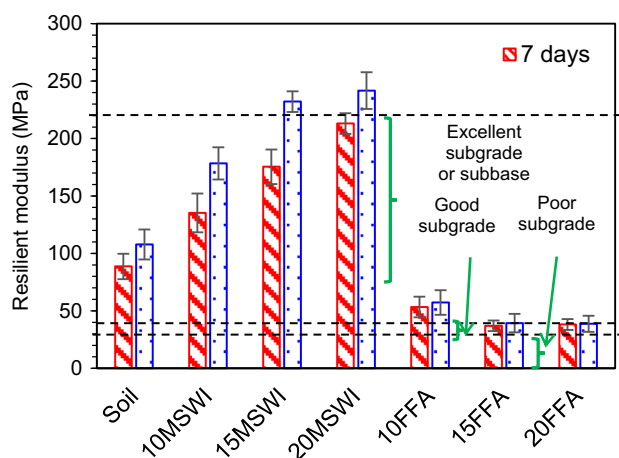


Fig. 9 Average resilient modulus after 7 and 28 days air curing

the resilient modulus of the clayey sample. Therefore, using FFA alone does not contribute to the resilient strength gain.

Based on the resilient modulus results, subgrade can be categorized as poor, good, and excellent [49]. AASHTO [5] recommends 42–228 MPa range for the subbase. Accordingly, control soil, 10MSWI, 15MSWI, 20MSWI, and 10FFA treated samples can be considered as excellent subgrade or subbase during the dry weather condition. Meanwhile, 15FFA and 20FFA samples are considered as good subgrade. Although, the average resilient modulus of the FFA stabilised subgrade is showing an acceptable range, they display a higher deformation. Therefore, FFA treated samples are not good as MSWI fly ash treated subgrades.

The results from the resilient modulus test were compared with the lime stabilised subgrade material. Mamatha and Dinesh [63] investigated the impact of adding 0–5% lime to black cotton soil. They found that the resilient modulus reached 243 MPa with 2% lime addition and 360 MPa with 3% lime addition after 28 days of water curing. Meanwhile, Bhuvaneshwari, Robinson and Gandhi [16] explored the resilient modulus of high plasticity clay with lime additions ranging from 0–8%. In their study, the resilient modulus measured 240 MPa for the sample with 4% lime addition and 250 MPa for the sample with 6% lime addition after 28 days of curing. Therefore, it could be concluded that the MSWI fly ash treated expansive clays perform as similar to the lime treated subgrades.

### 3.1.4 CBR

4-day and 10-day soaked CBR values of FFA and MSWI fly ash stabilised expansive clay samples are shown in Fig. 10. While the CBR of the control soil is negligible, the soaked CBR of the treated clays with MSWI fly ash improved drastically. MSWI fly ash treated clays exhibited 34%, 58%, and 62% CBR values with the addition of 10%, 15%, and 20% MSWI fly ash. However, no strength gain is observed for the FFA added soil samples and they exhibit zero CBR values. Although 10% FFA sample and control samples display a good compressive strength, their 4-day soaked CBR results are below 5%.

The Austroads guideline [12] suggests CBR greater than 5% can be used as subgrade material. Therefore, MSWI fly ash treated subgrade could be used to treat the soft clays which are more susceptible to moisture degradation. Clay samples treated with more than 10% of MSWI fly ash showed a CBR greater than 30%; thus, they can be used as a good subbase material. The soaked condition provides more water for the hydration reaction and creates more strong crystalline phases, which raises the sample strength. Therefore, compared to air curing, wet curing provides

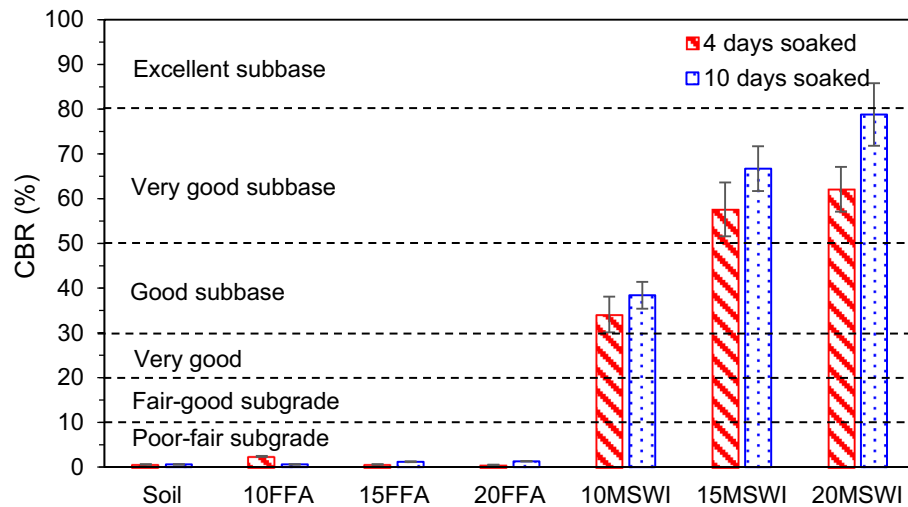


Fig. 10 Soaked CBR values after 4 and 10 days of curing

additional water for the hydration reaction. Also, in arid regions, MSWI fly ash stabilised soil gains more strength during flooding or other severe moisture fluctuation events.

The results for the 10-day soaked CBR show that the CBR of the MSWI fly ash stabilised clay increases by 12.6 (10MSWI), 15.8 (15MSWI), and 269 (20MSWI) percentages of the 4-day soaked CBR results of the same mix. Therefore, even for extreme weathering conditions, this MSWI fly ash can be used for the subgrade stabilisation of problematic clays. Figure 11 shows the samples after 10 days of soaking, and it can be observed that the samples become stronger with increased MSWI fly ash content. This strength gain is because of the increased pozzolanic reaction between clay and MSWI fly ash in the presence of water. Therefore, water curing is thought to be a more effective procedure in the field instead of air curing to achieve greater stiffness for MSWI fly ash stabilised subgrades/subbases. On the other hand, FFA is not suitable to treat the expansive clays which are exposed to moisture variations.

During the road design, subbase and base thicknesses are decided based on the CBR value of the subgrade. The greater the CBR value of a subgrade, the more carrying capacity it has to support the pavement. Therefore, a

thinner pavement thickness would be sufficient if the subgrade has a higher CBR value. Figure 10 shows the relative CBR values for subbase and subgrade requirement [49]. Based on the guideline, soil and FFA treated samples behave as poor-fair subgrade, whereas all the MSWI fly ash stabilised clays can be considered as a very good subgrade material. Besides, 15% and 20% MSWI fly ash treated samples can be used as a very good subbase material. UCS and resilient modulus values of the 10FFA treated samples were in the accepted range for the subgrade during the dry weather conditions. However, based on the soaked CBR results, FFA treated samples will not cope well during the seasonal rainfall events.

CBR of the lime treated expansive clay subgrades were compared with the CBR of MSWI fly ash treated samples. Kavak and Baykal [59] reported that the CBR for 4% lime-stabilized high-plasticity clay reached 55% after 7 days of soaking. Similarly, NASRIZAR and Muttharam [67] examined the performance of lime-treated expansive clay and found that the CBR value for 5% lime-treated clay was 31% when soaked under a curing temperature of 30 °C. Consequently, it can be deduced that samples stabilized with 15–20% MSWI fly ash exhibit CBR values within a similar range when compared to lime treated samples.



(a) Soil

(b) 20MSWI -10D soaked

(c) 20 FFA – 10D soaked

Fig. 11 Samples after 10 days soaking a soil b 20MSWI fly ash and c 20FFA

### 3.1.5 Moisture susceptibility

The loss of subgrade durability and bearing capacity due to the existence of moisture is referred to as moisture induced damage which results in reduced pavement life span. The extent to which subgrade mixture is prone to moisture damage is known as moisture susceptibility. Compressive strength results from the moisture susceptibility tests are presented in Fig. 12. Tests were conducted after the 7 days air curing and consequent immersion of the samples under water for 4 h. The control sample and FFA treated clays failed during the test, whereas MSWI fly ash stabilised samples showed no visual degradation after the soaking period. Compressive strengths of 10%, 15%, and 20% MSWI fly ash treated samples were 0.22, 0.27, and 0.29 MPa, respectively. FFA treated clays do not have much pozzolanic products and are highly porous. Therefore, water penetrates easily and reduces the cohesion and inter particle friction. Although, no visual defects were observed in the MSWI fly ash treated samples, there is a significant reduction in the compressive strength after the moisture susceptibility test. This strength reduction is attributed to the penetration of water into the micropores, which breaks the particle bonds thus losing the interparticle friction.

### 3.2 Wetting and drying test

Wet-dry tests were performed on the control sample of soil and 20MSWI fly ash stabilised samples (Fig. 13). The determination of 20% as the optimal ratio was based on a balance between achieving significant improvement in soil properties and maximising the MSWI fly ash usage. The control sample failed in the first wet cycle as it could not remain in the compacted state. However, UCS of 20MSWI fly ash stabilised sample increases after the first wetting–drying cycle and decreases in the following cycles, as

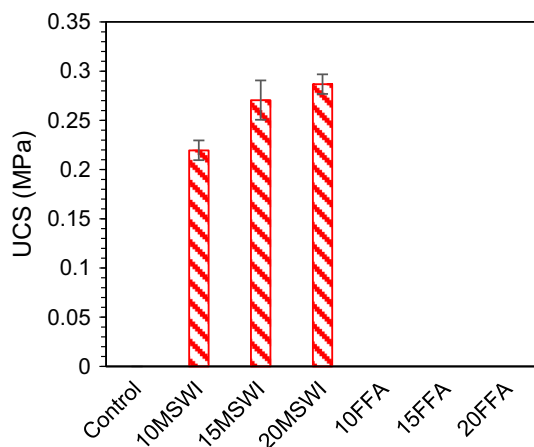


Fig. 12 UCS after moisture susceptibility test

shown in Fig. 14. The combined effect of MSWI fly ash solidification and control over expansion–shrinkage behaviour [101] enhances the soil's resilience to dry–wet cycles. The stabilized soil retains its structural integrity and mechanical strength even when subjected to fluctuating moisture conditions.

During the first wetting cycle, unreacted MSWI fly ash particles reacted with water and formed a greater number of pozzolanic products. Meanwhile, the first drying phase reduced the moisture by less than 5%, consequently increasing the sample's stiffness. Compressive strength increases from 0.86 MPa (7-day air cured sample) to 1.66 MPa after the first cycle, which is about two times. UCS then reduces to 1.35 and 0.86 MPa after the 3rd and 6th wet-dry cycles, respectively, about 19% and 48% of the compressive strength in the first cycle. During the first drying cycle, only minor cracks were formed. In the second wetting phase, water penetrated through those cracks, generating significant water pressure in the sample and destroying the pozzolanic bonds. The crack formation and water penetration in the subsequent wet-dry cycles further accelerated the degradation and reduced UCS.

After 6WD, samples were further soaked for 24 h and dried for 24 h (6WD + 24SD) to investigate the performance during long period of soaking. The UCS strength of the samples reduced slightly to 0.76 MPa. Similarly, another sample was soaked and dried for 48 h after the 6 WD (6WD + 48SD), and a slight increment in UCS (0.81 MPa) was observed compared to the 24h soaked and dried samples. Therefore, prolonged wetting and drying increases the UCS of MSWI fly ash stabilised soils due to the formation of many pozzolanic products, which partially repairs the cracks.

### 3.3 pH and heavy metal concentration

Soil pH is one of the critical factors in the soil stabilisation process. pH testing was conducted with water and  $\text{CaCl}_2$  for the control clay sample and 20MSWI fly ash stabilised samples, and the pH values in the water and  $\text{CaCl}_2$  varied  $\pm 0.5$ . The pH values of the soil were 8.29 and 8.56 in water and  $\text{CaCl}_2$  respectively, after 7 days of curing. The pH values were reduced to 8.15 and 8.49 in the same mediums after 28 days of air curing (Fig. 15). Therefore, soil can be considered alkaline, and the higher pH is due to the presence of exchangeable magnesium and sodium present in the soil.

The pH of the MSWI fly ash is 12.15 in both water and  $\text{CaCl}_2$ . When MSWI fly ash is added to the soil, pH increases from 8.3 to 10.3 for 7 days cured samples. MSWI fly ash has higher CaO content, and the addition of this fly ash increases the pH. Higher pH in the stabilised soil also increases the dissolution of silica and alumina and

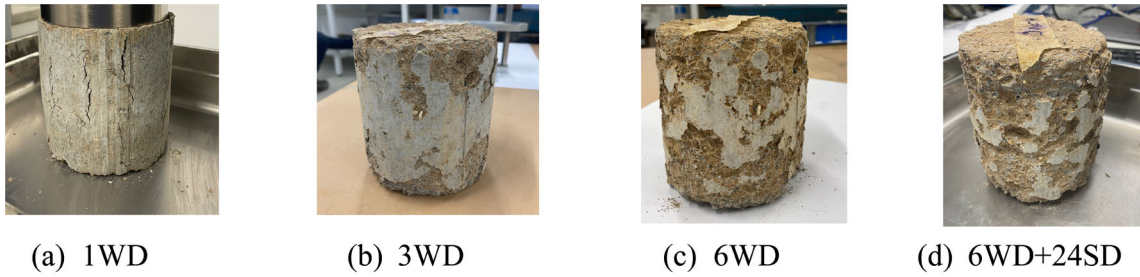


Fig. 13 Wetting drying samples after different weathering cycles

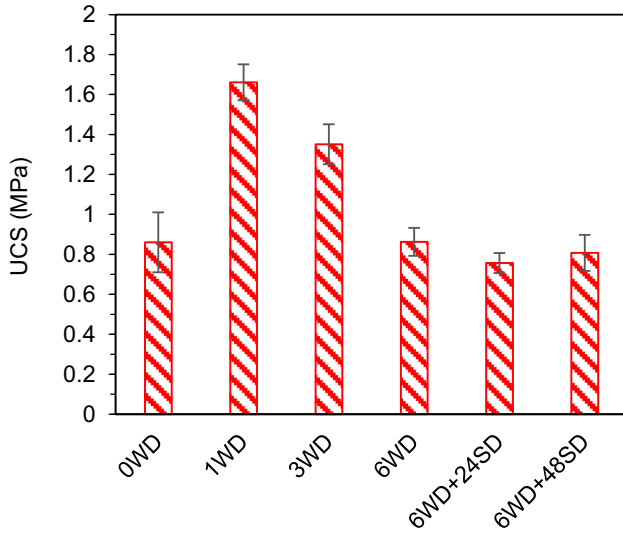


Fig. 14 UCS after wetting and drying cycles

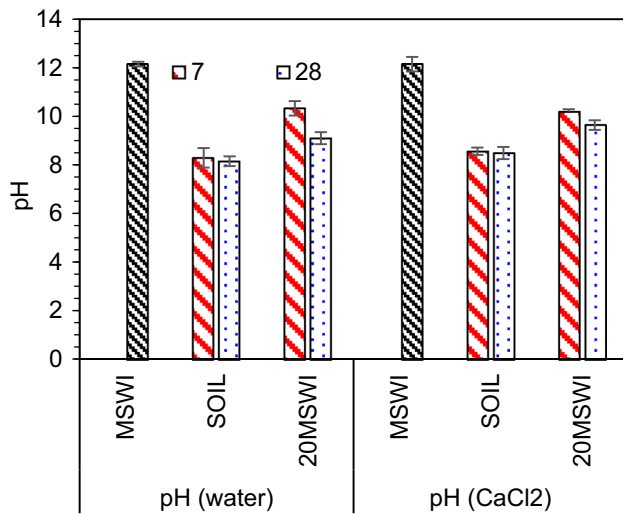


Fig. 15 pH after 7 and 28 days of curing

accelerates the pozzolanic chemical reaction [61]. Also, it increases the cation exchange capacity (CEC) of the soil, increasing particle aggregation [28, 42].

In addition to the pH tests, leachate analysis was conducted to evaluate the environmental impact from heavy

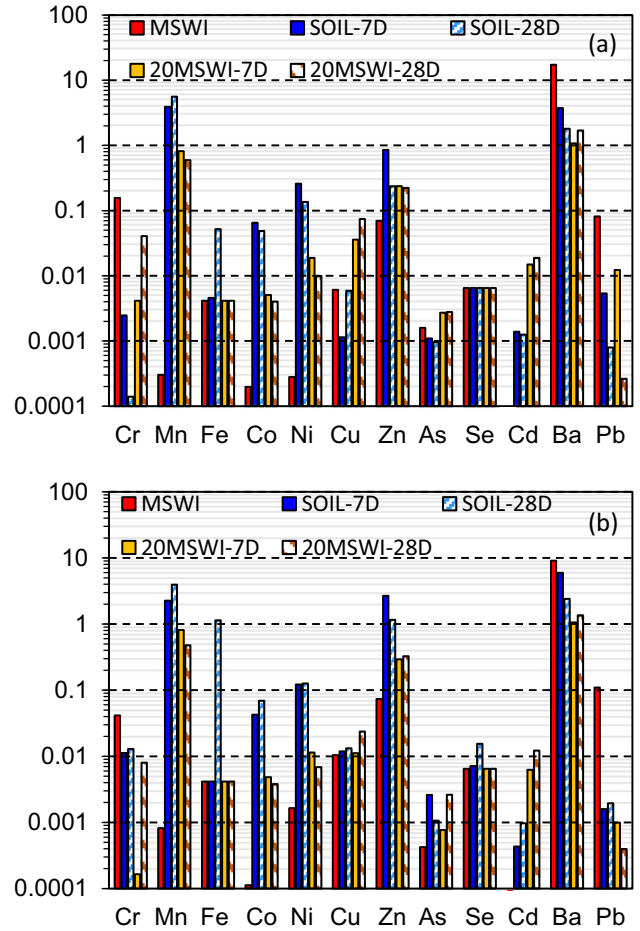


Fig. 16 Heavy metal concentrations after leaching with a pH 7 and b pH 5 buffers

metal leaching. Figure 16 shows the heavy metal concentrations of untreated and stabilised samples leached using pH 5 and 7 buffer after 7 and 28 days of curing. Leaching result of raw MSWI fly ash is also plotted as a comparison in Fig. 16.

Table 4 summarizes the maximum leaching concentration of metals from Fig. 16 and the maximum values for leachable concentration defined by various states in Australia. Allowable leachate limits defined by New South Wales [33], Western Australia [29], Victoria [35], South

**Table 4** Maximum heavy metal concentrations of tested samples and the maximum allowable state limits in Australia

	Maximum heavy metal concentration			NSW	Victoria	South Australia	Tasmania	Min (all states)
	MSWI fly ash	Soil	20MSWI	General solid waste	Category D/iIndustrial waste upper limit	Low level contaminated	Low-level contaminated soil	
Cr	0.15654	0.01292	0.04052	5	2.5	20	0.5	0.5
Mn	0.00082	5.60237	0.81699	–	–	50	25	25
Fe	0.00415	1.14114	0.00415	–	–	–	–	–
Co	0.00020	0.06913	0.00509	–	–	–	–	–
Ni	0.00165	0.25818	0.01882	–	1	2	1	1
Cu	0.01045	0.01320	0.07408	–	100	10	10	10
Zn	0.07364	2.66913	0.32517	–	150	250	25	25
As	0.00159	0.00260	0.00278	5	0.5	5	0.5	0.5
Se	0.00649	0.01543	0.00649	–	0.5	–	0.1	0.1
Cd	0.00006	0.00139	0.01885	1	0.1	0.5	0.1	0.1
Ba	17.30383	5.95979	1.69023	–	100	100	35	35
Pb	0.10969	0.00534	0.01229	–	0.5	5	0.5	0.5

Australia [32], and Tasmania [34] are included in Table 4. Table 4 also illustrates the least value of the heavy metal concentration from all the state-specified limits in the last column. The heavy metal concentration of the MSWI fly ash is within the allowable limit. 20MSWI fly ash treated samples exhibit a satisfactory level of heavy metal concentration which is within the maximum allowable limit mentioned by all the states in Australia.

Soil stabilization processes can contribute to the reduction of heavy metal concentrations through various mechanisms such as chemical immobilization, adsorption, and encapsulation during the pozzolanic process forming less soluble compounds. The encapsulation of heavy metal ions and enhanced binding to soil particles physically isolate them, preventing their release [22, 40]. By improving soil stability and structure, stabilization processes also minimize leaching, reducing the transport of heavy metals. Therefore, it is expected that no additional treatment process would be required to reduce the trace metal concentration of MSWI fly ash before any geotechnical application.

### 3.4 Microlevel analysis

#### 3.4.1 XRD

XRD testing was conducted to understand the phase change after mixing with fly ash stabilizers. The XRD analysis of the MSWI fly ash and FFA stabilised samples are shown in Fig. 17 after 7 and 28 days of curing in comparison with control soil. Figures 17a, b show the XRD results of the MSWI fly ash stabilised expansive clays after 7 and 28

days of curing. The main crystalline formations during the MSWI fly ash stabilisation are quartz (Q), gismondine (G), calcite (C), portlandite (P), andradite (D), and ettringite (E). Quartz is in 26.6°, 50.2°, and 60° angles, whereas gismondine [CaAl<sub>2</sub>Si<sub>2</sub>O<sub>8</sub>·4(H<sub>2</sub>O)] is identified in 20.8°, 26.7°, 33.2°, and 50.1°. Gismondine is a type of zeolite reported mostly in alkaline cementitious compounds [9, 41]. Portlandite is observed in 18°, 34.1°, and 50.8°, and the andradite phase is found in 33.2°, 57.1°, and 71.7°. Meanwhile, calcium phase is identified in 29.5°, 44°, and 64.5°. Moreover, ettringite is identified in 19°, 22.9°, 28°, 35°, and 49°. The XRD peak intensity of calcite and portlandite phases increased with the MSWI fly ash addition and curing duration. Higher ash content increases the potential for possible pozzolanic reaction and creates more crystalline bonds. Similarly, longer curing produces more hydrated products, improving the mechanical performance of the treated samples. The improved mechanical performance is evident with the UCS and resilient modulus testing results.

XRD diagrams of the MSWI fly ash treated clays after wet-dry (WD) cycles are shown in Fig. 17c. After the first WD cycle, the intensity of the ettringite, calcite and portlandite phases increases slightly. When the air-cured sample is exposed to water for the first time, unreacted MSWI fly ash particles in the sample react with water and form more cementitious bonds. However, the intensity of calcite and ettringite reduced after 3WD and 6WD cycles. During the third and sixth wet-dry cycle, the bond between hydration products breaks and the sample loses certain strength. UCS results also revealed that the sample's compressive strength is increased after the first weathering

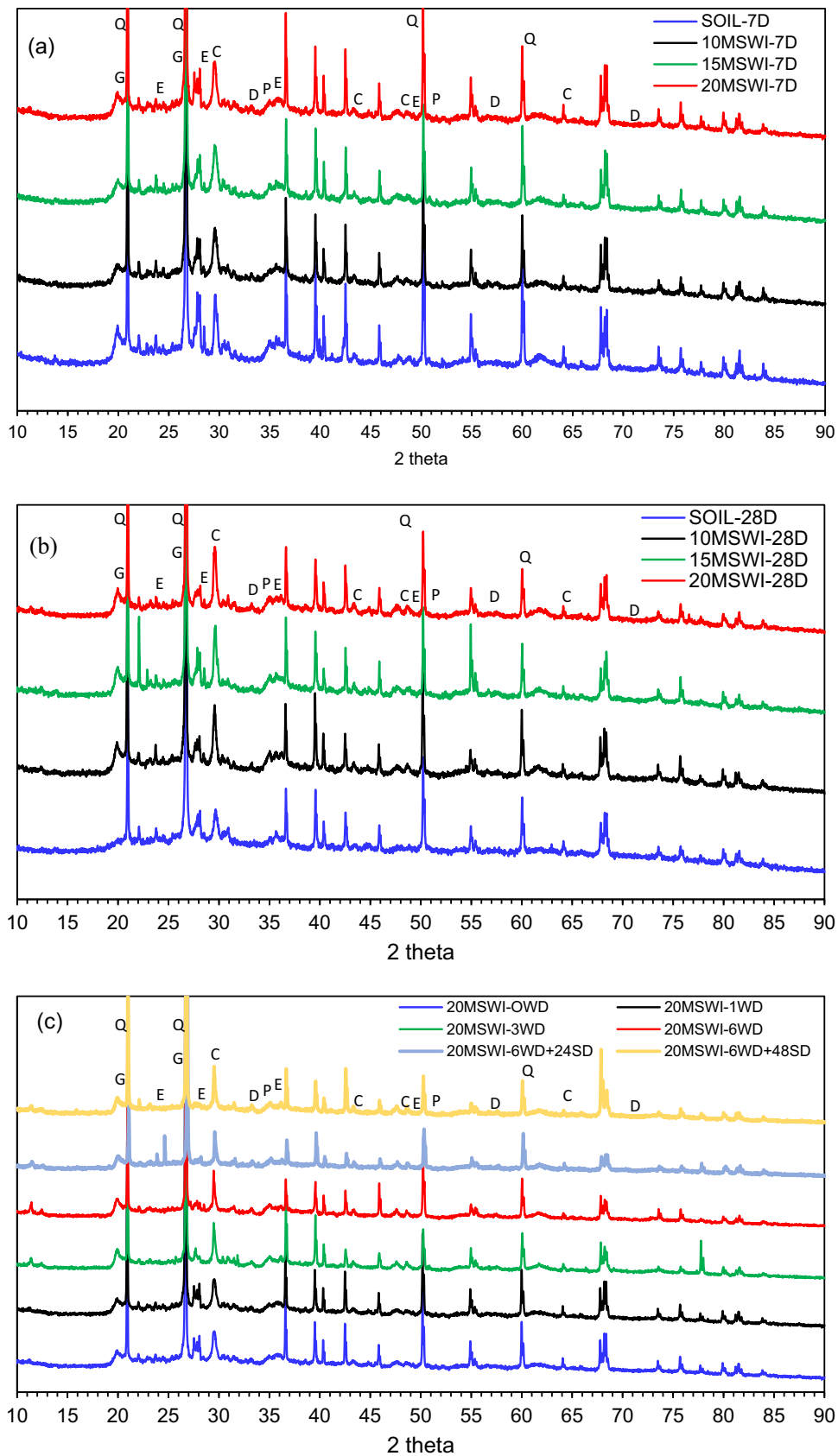
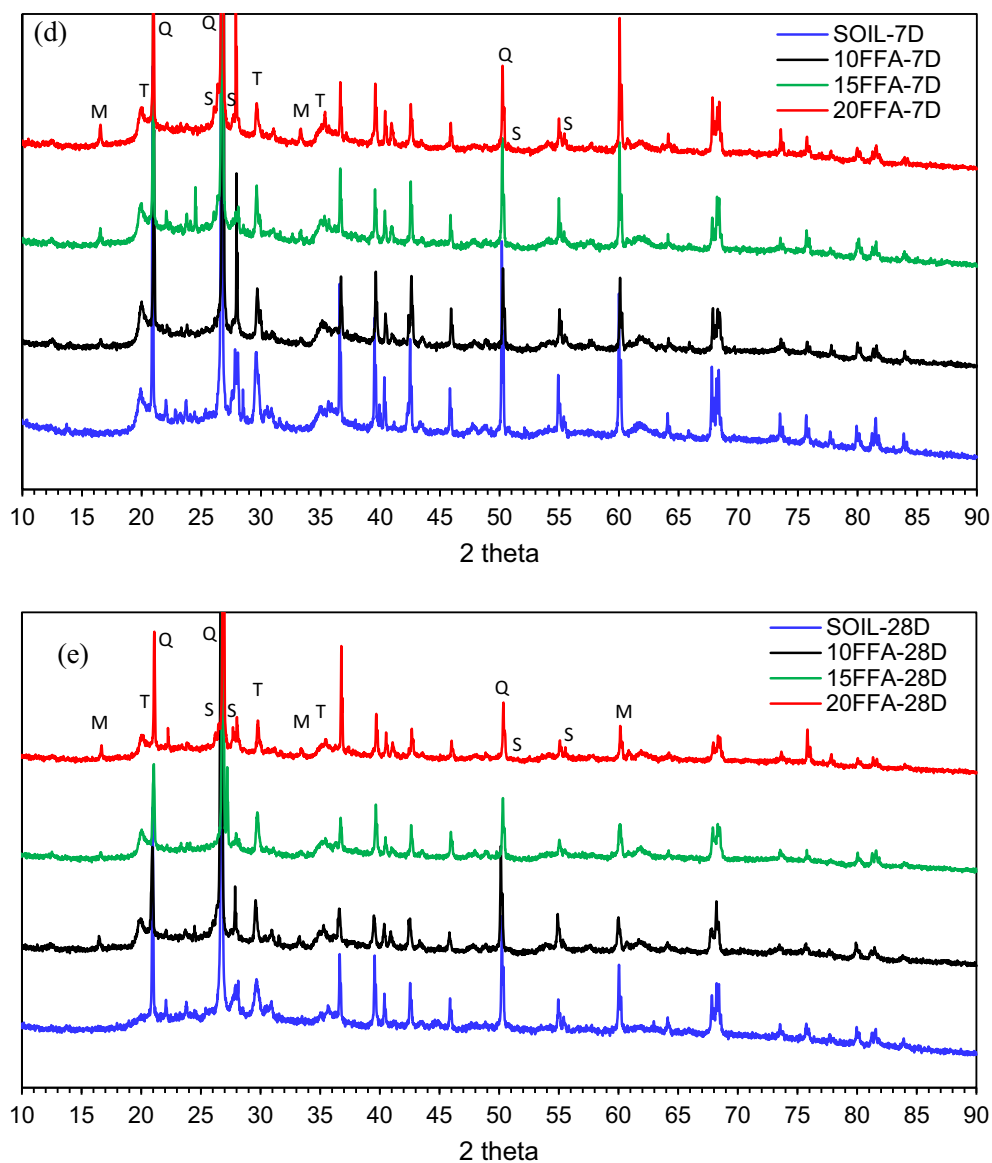


Fig. 17 XRD of the stabilised samples a MSWI-7D b MSWI-28D c Wet-dry samples d FFA-7D e FFA-28D



Q-Quartz, G-Gismondine, E-Ettringite, C-Calcite, D-Andradite, P-Portlandite, M-Mullite, T-Magnetite, S-Calcium Silicate Hydrate, CSH

Fig. 17 continued

cycle and then reduced in the 3rd and 6th wetting and drying cycles. 6WD + 24SD sample show only a very slight decrease in the peak intensities. However, the calcite phase is increased slightly during the long soaking period due to the formation of more pozzolanic products with the availability of CaO in the MSWI fly ash. A marginal increase in the calcite, portlandite, and ettringite phases can be observed after 48 h soak and drying (6WD + 48SD), which is also evident from the UCS test results. Prolonged wetting and drying forms a greater number of crystalline phases, which helps to gain certain strength. Therefore,

MSWI fly ash treated samples will perform well during an extreme flood event.

During the FFA stabilisation, quartz (Q), calcium silicate hydrate (CSH) (S), mullite (M), and magnetite (T) are identified as key phases. Quartz is present in  $21^\circ$ ,  $26.8^\circ$ , and  $50.5^\circ$ , while CSH is identified in  $21.1^\circ$ ,  $25.1^\circ$ ,  $27.3^\circ$ ,  $51.1^\circ$ , and  $55.7^\circ$ . Similarly, mullite is observed in  $16.3^\circ$ ,  $33^\circ$ , and  $60.1^\circ$  with higher peaks, whereas magnetite is observed at  $18.1^\circ$ ,  $29.7^\circ$ , and  $35^\circ$  angles. Similar crystalline phases are reported in other studies for the class F fly ash treated clays [89, 96]. It can be observed that the intensities of CSH, mullite, and magnetite are higher for the 10FFA



compared to the 15% and 20% FFA treated samples after 7 and 28 days curing. It can be clearly seen that the intensity of CSH is higher for 10FFA treated samples after 28 days curing. When FFA is added beyond 10%, they act as an unbound silt particle and does not react with water. Therefore, less hydration products are formed beyond 10% FFA addition and exhibit lower strength performance.

In summary, MSWI fly ash consists of higher CaO, thus, MSWI fly ash treated samples form higher number of portlandite phases which is reflected in the XRD spectrum. Although, SiO<sub>2</sub> is higher in the FFA, it has a very less amount of CaO (2.83%). Therefore, FFA treated samples do not create more hydration products.

### 3.4.2 FTIR

FTIR can be used to characterize individual hydration products and to understand the relative magnitude variation of the formation of these products under different curing and weathering conditions. The FTIR spectrum shows detector response, plotted in absorbance (%) vs wave number. Low absorbance reflects a few numbers of bonds to absorb at that frequency. In contrast, high absorbance means many bonds with similar vibrational energies of the incident light. FTIR diagram can be divided into two regions, absorption and fingerprint regions. Absorption bands correspond to the 4000–1500 cm<sup>-1</sup> region, and the fingerprint region is within 1500–500 cm<sup>-1</sup>. Absorption bands for inorganic materials can be observed in lower wave numbers in FTIR analysis due to their external crystalline matrix [27]. Some functional groups freely vibrate, and other groups' vibrations may be limited depending on the arrangement of molecules. This overall molecule arrangement pattern results in different vibrational bands in various wave numbers [27]. In the FTIR spectrum for both fly ash types, four absorption bands can be clearly distinguished; O–H stretching, O–H bending, C–O stretching, and Si–O stretching.

In Figs. 18a–e, control soil is plotted to compare the chemical effect after adding stabilisers. The absorbance at 3622 cm<sup>-1</sup> and 3696 cm<sup>-1</sup> in the untreated clay FTIR spectrum correspond to montmorillonite, which is attributed to the Al<sup>3+</sup> cations bound with the O–H group [19]. The doublet at 779 cm<sup>-1</sup> and 788 cm<sup>-1</sup> belongs to the crystalline mineral quartz [84]. During MSWI fly ash and FFA stabilisation, various changes occurred in the IR spectrum as explained below.

Figures 18a, b show the FTIR spectrum of MSWI fly ash stabilised soil after 7 and 28 days of curing. Absorbed water molecules on the sample surface produce broad O–H stretches in the 3150–3550 cm<sup>-1</sup> region. With the MSWI fly ash addition, more hydrated products form and increase the absorbance. Similarly, 28 days cured samples

absorbance increased compared to the 7 days cured MSWI fly ash treated clays. O–H bending occurs around 1640 cm<sup>-1</sup> [56, 95], and it can be detected in MSWI fly ash treated clays after 7 days of curing. A similar trend to O–H stretching can be observed for O–H bending for the MSWI fly ash treated samples.

Carbonates such as calcite show a strong absorption band from C–O stretching in the 1550–1350 cm<sup>-1</sup> region [27]. Calcite is an inorganic compound consisting of Ca<sup>2+</sup> cation and CO<sub>3</sub><sup>2-</sup> as the anion. Carbonate is a complex anion and a functional group that holds the anion tightly together due to its covalent bonds. These complex ions produce absorption bands which can be used to identify carbonates in the FTIR spectrum. Figures 18a, b show the C–O stretching near 1438 and 1442 cm<sup>-1</sup> for 7 and 28 days of cured MSWI fly ash treated samples. The peak intensity of the C–O stretching increased with the MSWI fly ash addition and the curing time. MSWI fly ash addition and curing time produce more CaCO<sub>3</sub> crystalline lattice structures, which increase the peak of the absorption band. Generally, higher cations tend to shift the absorption band to a lower frequency, which is evident in Fig. 18a, b. Absorption bands shift towards the left when the MSWI fly ash percentage is increased, which is attributed to the increase in cation concentration with the MSWI fly ash addition.

Silicates in the stabilised samples may exist in the form of amorphous silica or as crystalline silica. Crystalline silica does not react with water and forms hydrated products, however, amorphous silica is reactive and displays pozzolanic behaviour. MSWI fly ash has only a very small percentage of silica (6.72%). In the FTIR spectrum, amorphous silica produces Si–O bands near 1000–1100 cm<sup>-1</sup> [27, 56], whereas amorphous silica also exhibits vibrations closer to 1000 cm<sup>-1</sup>. Therefore, it is difficult to distinguish the amorphous and crystalline silica's Si–O stretching during soil stabilisation as the soil has a higher percentage of crystalline silica.

Si–O absorption band for MSWI fly ash treated clays can be observed near 1000 cm<sup>-1</sup> (Fig. 18). Also, Fig. 18 shows a slight decrease in peak intensity with the MSWI fly ash addition, and the band peak increased higher than soil after 7 days of curing. As the MSWI fly ash has lower SiO<sub>2</sub>, the formation of calcium silicate hydrate may not be significant. However, a slight increase in Si–O stretching is observed in 1000 cm<sup>-1</sup> for the 20% MSWI fly ash treated clays. This increment could be attributed to the CSH formation with the higher percentage of MSWI fly ash, which may have provided enough SiO<sub>2</sub> to the samples. In 28 days of air curing time, a slight increase in the Si–O stretching band could be observed for the 10% and 15% of MSWI fly ash treated clays. Therefore, longer curing times create

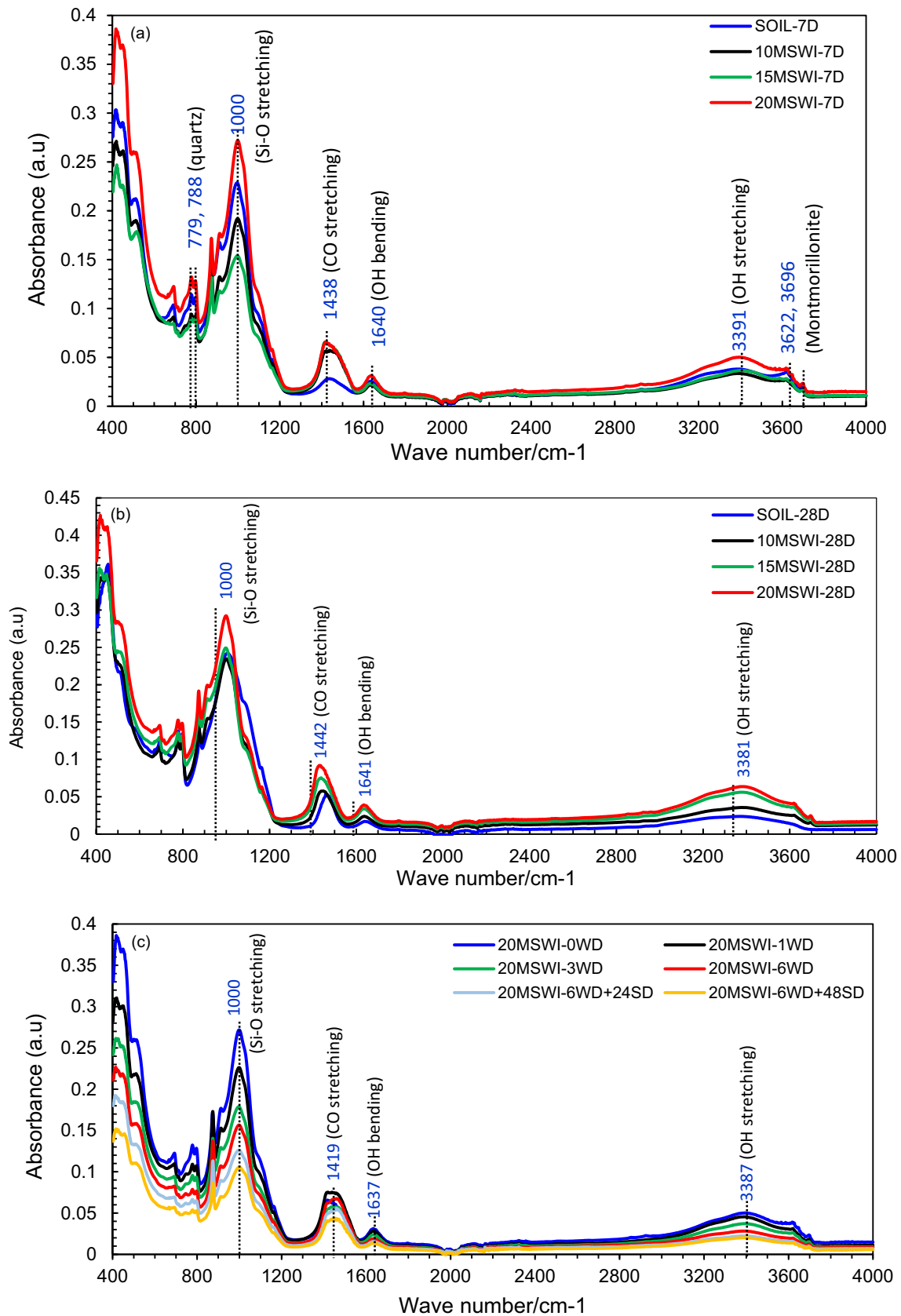


Fig. 18 FTIR spectrum of the stabilised samples **a** MSWI-7D **b** MSWI-28D **c** Wet-dry samples **d** FFA-7D **e** FFA-28D

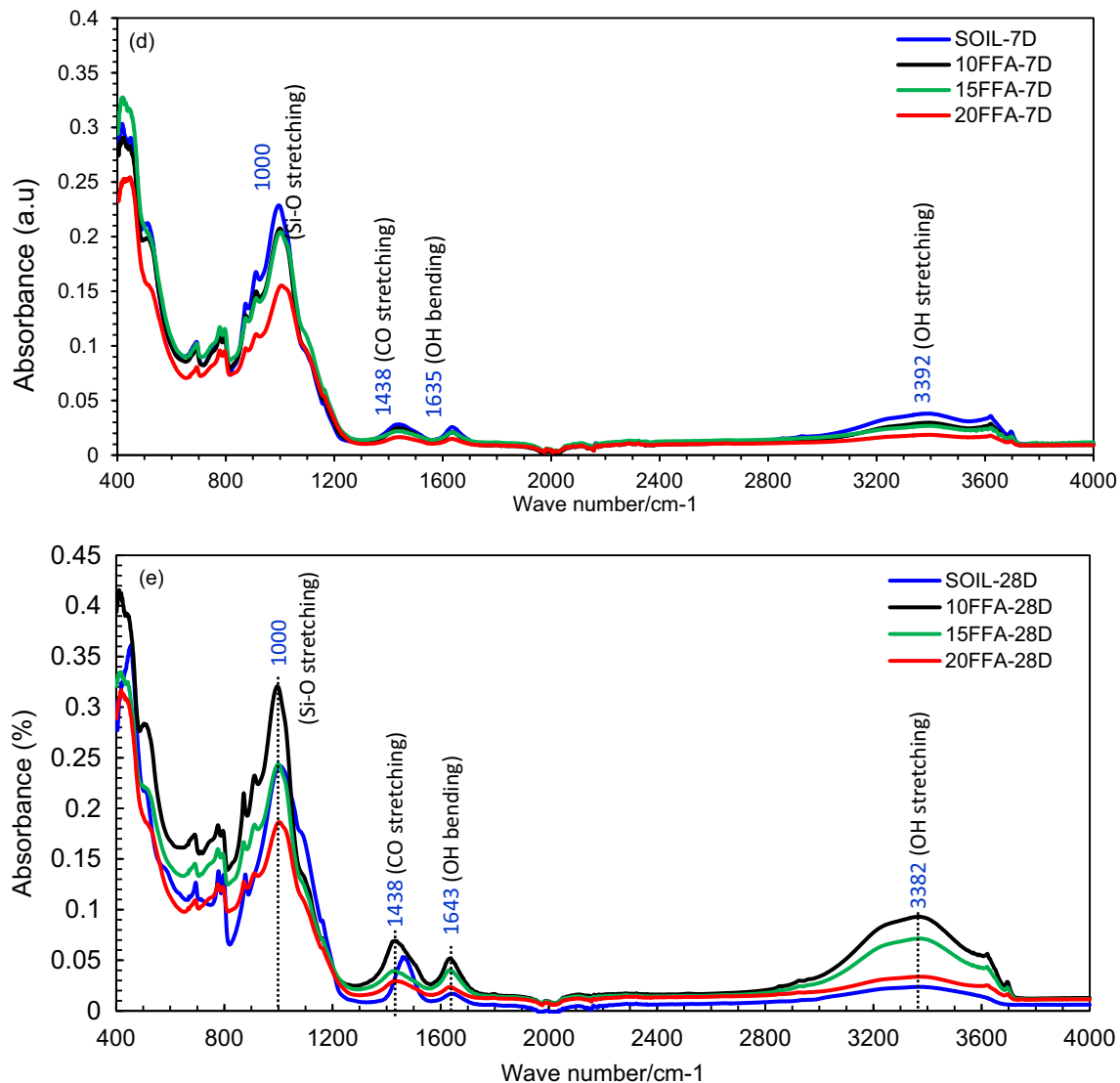


Fig. 18 continued

more silicate hydrates and increase the peaks for all the MSWI fly ash treated samples.

Figure 18c shows the IR spectrum after the wetting and drying weathering cycles. It can be seen that the O–H stretching peaks reduced slightly with the number of weathering cycles. Weathering cycles break the crystalline hydrated products, which reduce the peak intensities. Absorption bands of C–O stretching reduce as similar to the OH stretching with the cyclic wetting and drying process. The wetting and drying process destroys the calcite crystalline structures, consequently lowering the peak intensity. It can be also observed that the peak intensity of Si–O stretching of the MSWI fly ash stabilised clays reduced as similar to the O–H and C–O stretching.

FTIR diagrams of the FFA treated clay samples are shown in Fig. 18d, e after 7 and 28 days of curing. FFA

treated clays exhibit O–H stretching at 3392 cm<sup>-1</sup> and 3382 cm<sup>-1</sup> after 7 and 28 days of curing. FFA treated samples do not show a very significant peak after 7 days of curing. However, peak intensities increased for the 10% and 15% FFA stabilised clays. 20FFA treated samples showed no considerable peaks after 7 or 28 days of curing. O–H bending can be detected in FFA treated clays in 1635 cm<sup>-1</sup> after 7 days of curing. The peak intensity of the C–O stretching is smaller after 7 days of curing, and a slight increment can be noticed after 28 days of curing. FFA has a smaller percentage of CaO; thus, calcite formation is insignificant. In 28 days of curing, 10% of FFA treated samples exhibit a higher peak intensity than the other FFA treated samples in the C–O stretching region. Beyond 10% FFA, fly ash does not produce much calcite and remains in the mix without reacting, which is further

evident from the UCS and resilient modulus testing results (Figs. 6 and 9).

Figures 18d, e show the Si–O stretching of the FFA treated samples after 7 and 28 days of curing. The influence of crystalline silica in the soil is higher in 7 days of curing, resulting in a higher peak for the soil sample than the FFA treated soils. 20FFA treated clay exhibits a lower Si–O stretching compared to the 10% and 15% FFA added samples. Therefore, FFA added beyond 15% does not contribute to the CSH formation, and they act as unreacted silty fly ash, which subsequently reduces the intensity of the peak band. After 28 days curing, 10FFA treated samples display a higher peak intensity compared to the other samples as shown in Fig. 18e. This increment means that the 10% FFA addition creates more CSH during the long curing period and increases the UCS (Fig. 6) of the treated clays.

Overall, FTIR results reveal the occurrence of Si–O stretching, C–O stretching, O–H bending, and O–H stretching during the MSWI fly ash and FFA addition. The absorbance intensities of these bond stretching/ bending are higher for the MSWI fly ash treated samples than the FFA modified specimens. Also, there is a slight increment in the peak absorbance with the curing time for both MSWI fly ash and FFA stabilised samples.

### 3.4.3 TGA

TGA analysis quantifies gaseous emissions by measuring the mass loss of a sample subjected to a steady temperature increase. Each phase in the TGA diagram is assessed by its specific mass loss in the particular temperature range. These diagrams are helpful in understanding dihydroxylation and hydration processes during the soil stabilisation process. Figure 19 shows the TGA diagrams of stabilised samples and Table 5 summarizes the mass loss during the heating process.

Figures 19a, b show the TGA and DTG (Derivative Thermogravimetry) curves of the MSWI fly ash stabilised samples after 7 and 28 days of curing. The sharp decrease in mass between 40–105 °C is due to the vaporization of unbounded water on the surface [50, 99]. The mass loss from 105 to 200 °C occurred due to the desorption of interlayer water moisture trapped between clay particles linked to cationic exchange [7, 74]. Overall mass loss of the 7D and 28D cured samples are almost similar and equal to 15.6%. The peak around 400 °C is due to the dihydroxylation of kaolinite which typically occurs within 430–450 °C range [86, 88].

After MSWI fly ash was added to the soil, several phase changes were identified in the TGA results which were also reflected in the XRD analysis. All the MSWI fly ash treated samples consist of soil; therefore, the decomposition

experienced by the MSWI fly ash also has a similar pattern. However, in addition, several changes could be observed in Fig. 19a, b. TGA/DTG results of the MSWI fly ash stabilised samples (Fig. 19a, b) show three major endothermic peaks in the range of 30–200 °C, 360–520 °C, and 650–720 °C. Mass loss between 30–200 °C temperatures is due to the loss of interlayer water and dehydration of ettringite and gismondine phases [70, 73, 74]. During the 7 days of curing, mass loss of the treated samples slightly reduces with the fly ash addition. Loss of interlayer water influences the mass loss more than the dehydration of gismondine and ettringite phases. After 28 days of curing, mass loss in the 30–200 °C region increased than the 7 days cured samples. This increment can be attributed to the formation of a greater number of hydration products such as gismondine and ettringite with the curing. Mass loss for 20% MSWI fly ash treated soil increased from 4.57% (7D) to 8.5% (28D). The peak towards 360–520 °C corresponds to the dehydration of portlandite, and the mass loss increases with the higher MSWI fly ash percentage for the 7 and 28 days cured samples, highlighting its increased presence in the treated clay. The peaks at 650–720 °C are due to the decomposition of calcite, which is not much significant in 7 days of curing. After 28 days of curing, mass loss dramatically increased with the MSWI fly ash addition. The mass loss increased from 0.72% (control) to 8.81% for the 20MSWI fly ash treated samples in the 650–720 °C region (Table 5).

Figure 19c shows the TGA of the 20MSWI fly ash treated samples after undergoing several wetting and drying cycles. Mass loss of stabilised samples increase from 4.57% (control) to 7.14%, 7.11%, and 6.91% after 1, 3, and 6 cycles within 30–200 °C temperature range (Table 5). During wet-dry cycles, samples were submerged in the water for 6 h and oven dried at 70 °C for 42 h. Therefore, more absorbed water present in the wet-dry samples, increases the mass loss. The mass loss was further reduced to 6.52% for the 6WD + 24SD sample. A slight increment in mass loss can be seen for the 6WD + 48SD sample, which may be due to sample absorbing water during the long soaking period. The mass loss between 400–520 °C is due to the dehydration of the portlandite phase. After the wetting and drying, mass loss of 20MSWI fly ash treated samples reduced from 3.15% (Control-20MSWI) to 2.88%, 2.49%, and 2.47% in 1, 3, and 6 wetting-drying cycles, respectively. On the other hand, mass loss slightly increased for the 6WD + 48SD sample. During the prolonged soaking, sample absorbs water and reacts with MSWI fly ash and forms more portlandite crystalline structures, which results in higher mass loss. Calcite decomposition occurs in between 600–700 °C during the wetting and drying cycles. A slight increment in the mass loss can be observed till three wet-dry cycles.

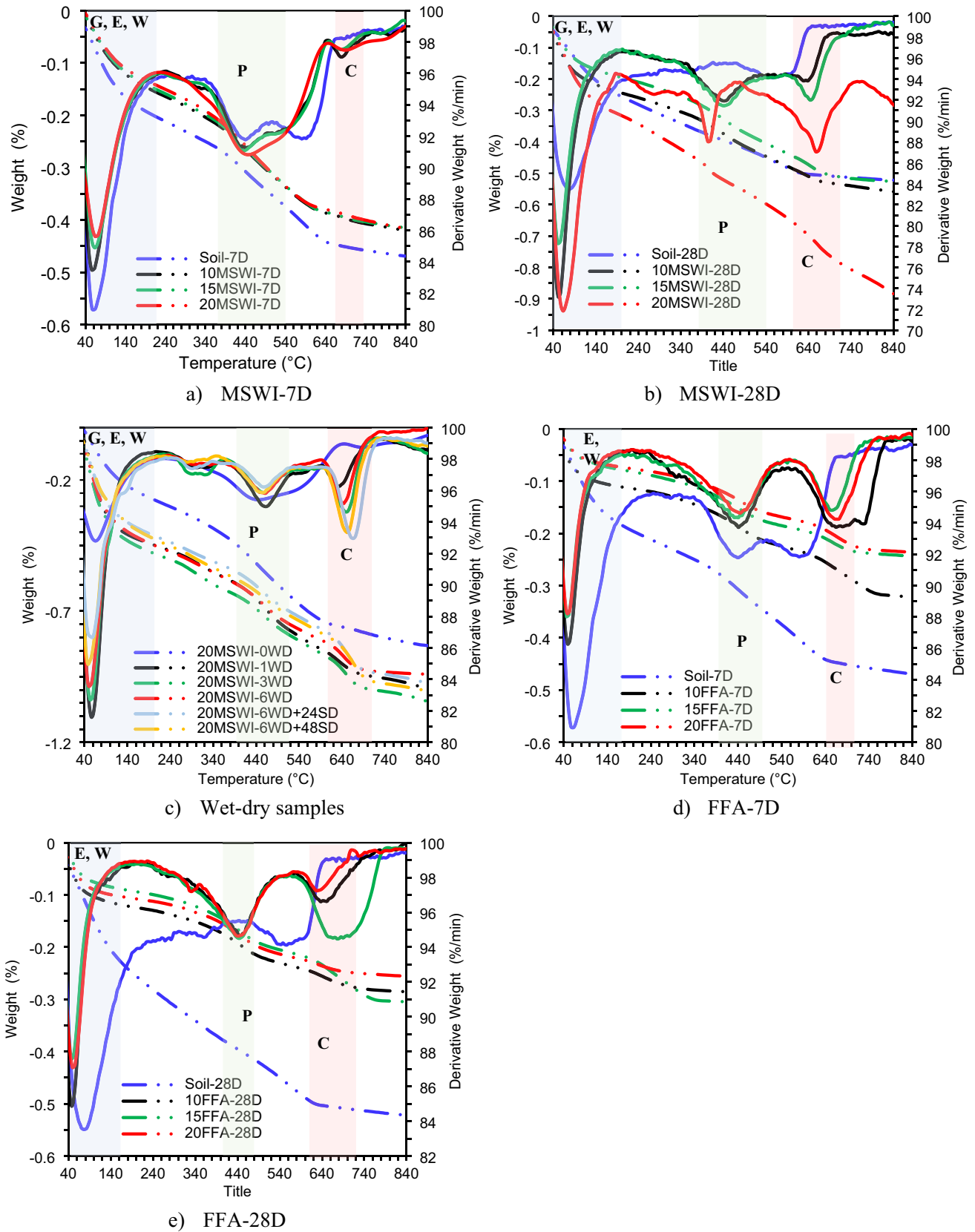


Fig. 19 TGA/DTG of the stabilised samples a MSWI-7D b MSWI-28D c Wet-dry samples d FFA-7D e FFA-28

**Table 5** Mass loss (%) with the temperature change

	Gismondine, Ettringite, Water	Portlandite	Calcite		CSH, Water	Portlandite	Calcite
<b>Temp (°C)</b>	<b>30–200</b>	<b>360–520</b>	<b>650–720</b>	<b>Temp (°C)</b>	<b>30–200</b>	<b>380–500</b>	<b>620–720</b>
SOIL-7D	5.73	3.43	0.38	10FFA-7D	2.57	1.86	1.75
10MSWI-7D	4.88	3.69	0.65	15FFA-7D	2.31	1.73	1.14
15MSWI-7D	4.7	3.77	0.48	20FFA-7D	2.18	1.62	1.55
20MSWI-7D	4.57	3.98	0.52				
<b>Temp (°C)</b>	<b>30–200</b>	<b>360–520</b>	<b>600–720</b>	<b>Temp (°C)</b>	<b>30–160</b>	<b>380–520</b>	<b>600–760</b>
SOIL-28D	7.55	2.54	0.72	10FFA-28D	2.76	1.85	1.17
10MSWI-28D	7.14	3.57	1.59	15FFA-28D	2.29	1.96	2.43
15MSWI-28D	5.21	3.75	2.11	20FFA-28D	2.28	1.91	0.81
20MSWI-28D	8.5	4.23	8.81				
<b>Temp (°C)</b>	<b>30–200</b>	<b>400–520</b>	<b>600–700</b>				
20MSWI-0WD	4.57	3.15	0.73				
20MSWI-1WD	7.14	2.88	1.58				
20MSWI-3WD	7.11	2.47	2.13				
20MSWI-6WD	6.91	2.49	1.83				
20MSWI-6WD + 24SD	6.52	2.45	2.56				
20MSWI-6WD + 48SD	6.54	2.8	1.93				

After three wet-dry cycles, mass loss slightly reduces, which may be due to the breaking of calcite crystalline structures during the continuous wetting and drying. However, a small increase in mass loss can be seen for the 6WD + 24SD sample. Long soaking period provides more moisture to the sample and facilitates the formation of more calcite crystalline products.

Figures 19d, e display the TGA/DTG of the FFA treated clays and Table 5 shows the respective mass loss (%) in different temperature ranges. There are three distinguished phases in the diagram which are due to the dehydration of CSH, water, and portlandite and decomposition of calcite. Mass loss in between 30–200 °C and 30–160 °C at 7 and 28 days curing are due to the evaporation of water and dehydration of CSH phases. Optimum moisture content of the FFA stabilised samples reduced with the FFA addition (Fig. 5). Therefore, loss of water in 30–200 °C region reduces with the FFA increment. However, compared to the MSWI fly ash, mass loss in this region is less for FFA treated samples. This is because FFA consists of a small percentage of CaO which is not sufficient to form higher number of pozzolanic products. Therefore, only slight mass loss is observed in the 30–200 °C region which is mainly due to the water evaporation. Mass loss in the 380–520 °C region is due to the dehydration of portlandite phase. Nonetheless, there is no any notable trend with the FFA addition after 7 and 28 days curing. Due to the calcite decomposition, mass loss occurs in 600–760 °C region. After 7 days curing, mass loss is higher for the 10FFA compared to 15FFA and 20FFA treated samples. Mass loss

is very small for the 20FFA sample compared to the 10% and 15% FFA treated samples. Therefore, it can be concluded that the 10FFA treated samples have performed well compared to the 15FFA and 20FFA samples. This is also reflected in UCS results which revealed that the 10% FFA treated clays achieved higher strength compared to the other samples (Fig. 6). Overall, TGA/DTG clearly explains the phase changes during the soil stabilization process using MSWI fly ash and FFA.

#### 3.4.4 SEM

Microscopical analysis was conducted on control, stabilised, and wet-dried samples to understand the underlying mechanism of the stabilisation process on a micro-scale. SEM images of MSWI fly ash and FFA stabilised samples are shown in Figs. 20 and 21 after 7 and 28 days of curing time. Untreated expansive clay soil exhibits flaky-shaped particles with more visible discontinuous pore structures without any hydration products, and the pore size increases with the curing time. This pore size increment is due to the loss of moisture from the soil with time. SEM images show a significant change in the pore structure distribution after the clay is treated using the MSWI fly ash and FFA.

MSWI fly ash stabilised samples show a stronger, tightly packed bond, having tiny pores. During the initial mixing stage, the influence of cationic exchange is more decisive and flocculates the soil particles. Hydration reaction occurs then and forms a stronger crystalline product. SEM images of the MSWI fly ash stabilised samples display the

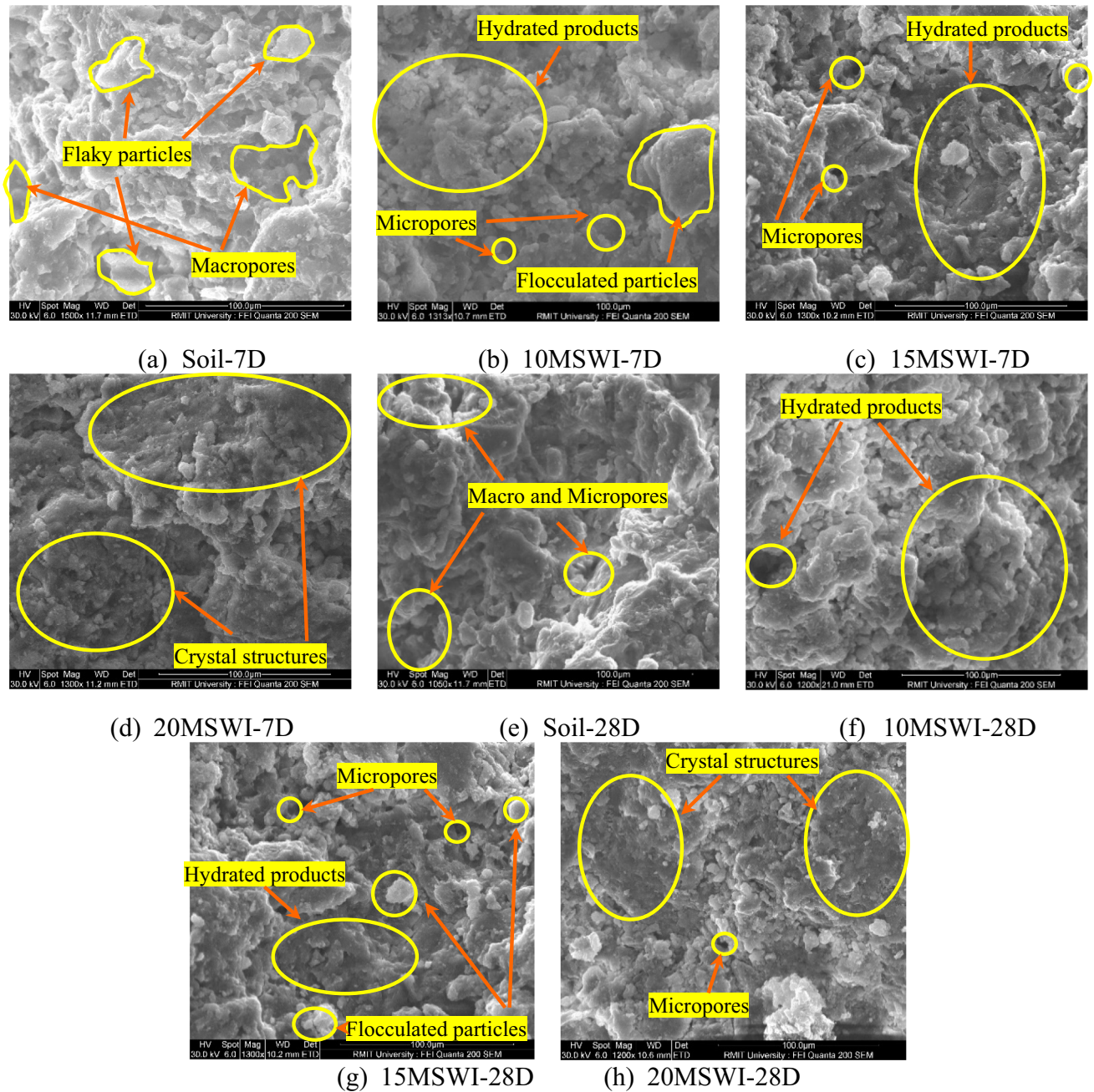


**Fig. 20** SEM of MSWI fly ash stabilised soils **a** Soil-7D **b** 10MSWI-7D **c** 15MSWI-7D **d** 20MSWI-7D **e** Soil-28D **f** 10MSWI-28D **g** 15MSWI-28D **h** 20MSWI-28D

agglomerated and hydrated particles, which reduce the pore size and produce a firmly bonded dense structure. MSWI fly ash has a higher percentage of CaO (52.6%), that enables the formation of a large number of crystalline structures. With the MSWI fly ash increment, more pozzolanic reactions occur, and the samples become stronger. This is also revealed via the XRD results of the MSWI fly ash stabilised samples that showed the formation of gismondine, albite, calcite, portlandite, andradite, and ettringite crystalline phases filling the voids thereby creating

denser samples. Also, enhancement in cement hydration products is confirmed in Fig. 20f–h with 28 days of air curing. Microscopical observations are consistent with the mechanical testing results (Figs. 6, 9, and 10).

SEM images of the FFA stabilised samples are shown in Fig. 21. SEM image of 10FFA treated sample indicates a smooth surface and a good bonding between particles. Beyond 10% FFA addition, fly ash is not reacting with the soil and water, and many non-dissolved FA can be observed. The surface morphology of FFA stabilised

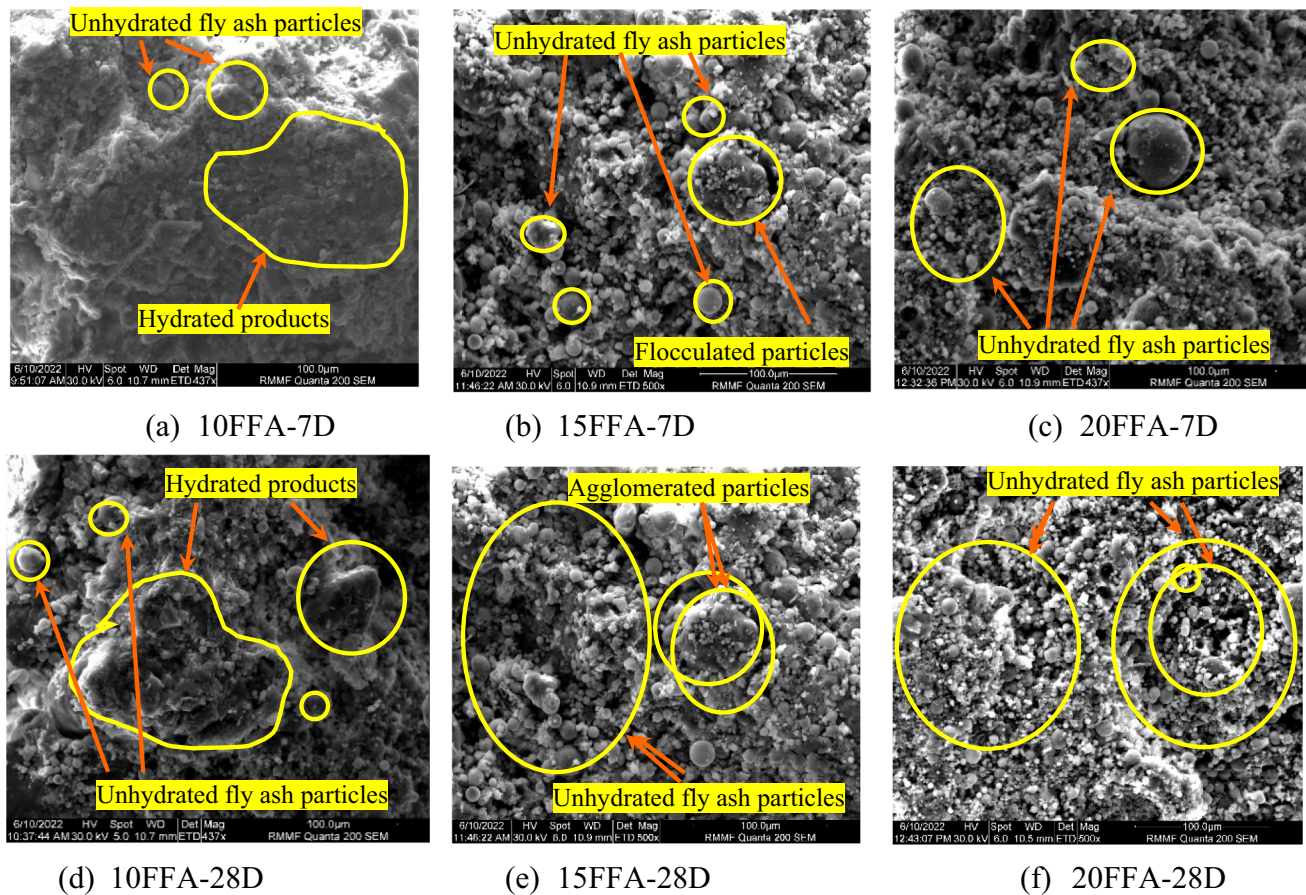


**Fig. 21** SEM of FFA stabilised soils **a** Soil-7D **b** 10FFA-7D **c** 15FFA-7D **d** 20FFA-7D **e** Soil-28D **f** 10FFA-28D **g** 15FFA-28D **h** 20FFA-28

samples show several untreated spherical fly ash particles. FFA has a very small amount of CaO and a higher percentage of SiO<sub>2</sub>; thus, it does not form a robust crystalline cement matrix. With the curing, 10FFA treated soil only shows a bonded crystalline structure, whereas other samples have a higher number of unreacted FFA particles.

Figure 22 shows the SEM images after wetting and drying weathering cycles. MSWI fly ash stabilised samples were tested after different number of weathering cycles. Particle morphology, structural surface characteristics, and pore distribution changed significantly after wet-dry (WD) cycles. After WD cycles, the bond between soil and stabiliser weakened and cracks formed. After wetting and drying cycles, cracks propagate and separate the particles. WD cycles increase the pore size gradually. Crack propagation increases with the WD processes. However, it can be seen that the MSWI fly ash treated samples performed well even after 6 WD cycles. It can be observed from the UCS test results that the strength of the stabilised sample is reduced slightly after the WD cycle testing. This degradation is due to the phase change of minerals and

microstructure change. It indicates that although there is a slight reduction in the stabilised sample's strength performance, MSWI fly ash stabilised samples perform well during the weathering process.

#### 4 Conclusions and recommendations

This study discusses the effect of municipal solid waste incineration (MSWI) fly ash and coal fly ash (FFA) to treat high plasticity expansive clays (CH) in pavements. These fly ashes were mixed with clay in various proportions (10%, 15%, and 20%) and a series of tests was conducted to understand the mechanical, durability, and environmental performance. Moreover, micro-level investigations such as XRD, FTIR, TGA, and SEM were conducted to understand the stabilisation mechanism of these fly ashes. Based on this detailed study, the following conclusions and recommendations can be drawn;

1. MSWI fly ash contains more irregular unbound carbons and fewer hollow spheres as compared to the



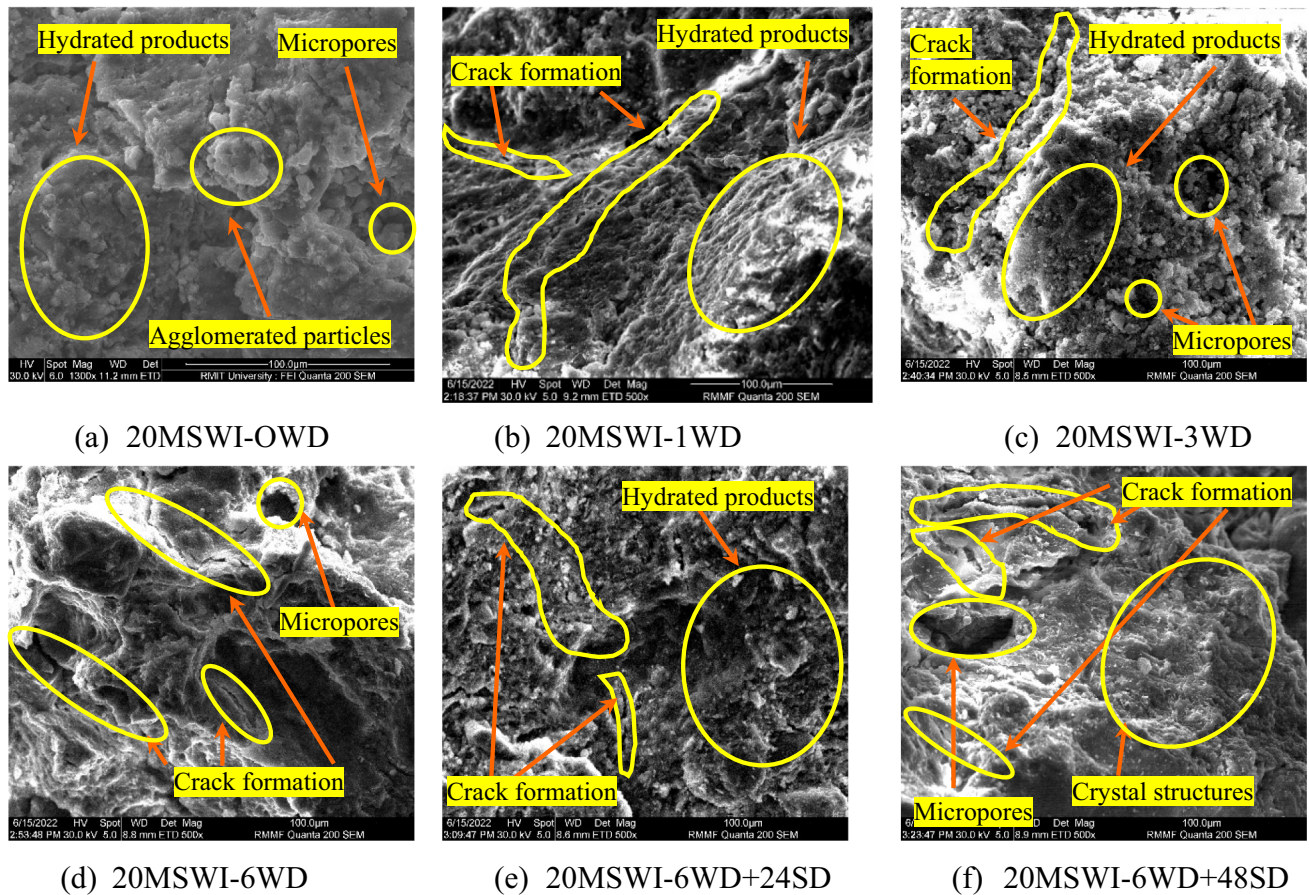


**Fig. 22** SEM images of wet-dried samples **a** 20MSWI-0WD **b** 20MSWI-1WD **c** 20MSWI- 3WD **d** 20MSWI-6WD **e** 20MSWI-6WD + 24SD **f** 20MSWI-6WD + 48SD

FFA. The major oxides in MSWI fly ash are CaO, SiO<sub>2</sub>, Al<sub>2</sub>O<sub>3</sub>, TiO<sub>2</sub>, Fe<sub>2</sub>O<sub>3</sub>, and MgO, whereas FFA consists of SiO<sub>2</sub>, Al<sub>2</sub>O<sub>3</sub>, Fe<sub>2</sub>O<sub>3</sub>, and CaO. MSWI fly ash stabilisation showed good performance compared to FFA due to the greater CaO/SiO<sub>2</sub> and CaO/(SiO<sub>2</sub> + Al<sub>2</sub>O<sub>3</sub>) ratios of 7.8 and 4.8, respectively, whereas FFA had only 0.06 and 0.04 in corresponding ratios.

- Maximum dry density (MDD) of the stabilised samples decreased with the MSWI fly ash addition and increased for FFA. During the early stages of stabilisation, the influence of cation exchange is more decisive in the MSWI fly ash-treated clays due to the presence of higher Ca<sup>2+</sup> ions, which increase the total volume and reduce the MDD. However, the impact of hydration is higher for the FFA stabilised samples in the early stages, which increases the MDD by filling the soil voids.
- Compressive strength and resilient modulus of the treated samples increased with the MSWI fly ash addition. 20% MSWI fly ash treated sample exhibited 0.86 and 2 MPa after 7 and 28 days

curing, respectively, while the resilient modulus of the treated clay increased from 89 MPa (control soil) to 213 MPa in 7 days curing. FFA treated samples did not exhibit significant strength beyond 10% addition. 10% FFA treated sample showed 1.1 and 1.2 MPa compressive strength after 7 and 28 days of curing, respectively. However, all the FFA treated clays displayed a poor resilient modulus and a larger deformation.

- Durability performance was investigated using soaked CBR and moisture susceptibility testings. MSWI fly ash treated samples showed an excellent performance during the soaked CBR (4D & 28D) and moisture susceptibility testing, while the control and FFA treated samples failed during the test.
- Wetting and drying test results of the optimum mix (20MSWI) showed that the samples were durable even after 6 wet dry cycles, followed by 48 h soaking and drying.
- Leachate testing results from MSWI fly ash treated soil revealed that the heavy metal concentrations in pH 5 and 7 after stabilisation are within the

maximum allowable limits mentioned by different states in Australia.

7. XRD results showed that the main crystalline formations during the MSWI fly ash stabilisation are quartz, gismondine, albite, calcite, portlandite, andradite, and ettringite. Meanwhile, FFA stabilisation forms quartz, calcium silicate hydrate, mullite, and magnetite crystalline structures. FTIR and TGA results confirmed the presence of portlandite, calcite, and ettringite phases. Microlevel analysis showed that the intensity of peak increased with curing time and MSWI fly ash addition, while only 10% FFA showed a significant change. Also, SEM images after stabilisation and during weathering cycles further confirmed the stabilisation mechanism and crack formation during weathering cycles.
8. Overall, 15% and 20% MSWI fly ash treated subgrades perform well for dry and wet weather conditions. However, 10% MSWI fly ash and 10% FFA modified subgrades can be used if the weathering condition is dry.
9. The performance of MSWI fly ash stabilized clays depict comparable results to that of conventional stabilizers used in the literature. The performance of MSWI fly ash in expansive clays can be further compared with the widely used additives such as lime and cement in future studies.
10. Suitability of MSWI fly ash for expansive soil stabilization may vary depending on the specific characteristics of the fly ash and soil involved. Therefore, while our study demonstrates its effectiveness in this context, it is recommended to evaluate the applicability of MSWI fly ash on a case-by-case basis, considering the source and composition of the fly ash and the properties.

This study provides an insight into the expansive clay stabilisation using industrial waste ash for the potential improvement of pavement performance. Based on the mechanical, durability, and micro-level investigations, MSWI fly ash based stabilisation is effective to improve the durability of the expansive clay soil without causing excessive leachates. The outcomes from this project are expected to benefit practitioners with the provision of a sustainable road construction strategy and help authorities resolve a growing solid waste catastrophe.

The use of MSWI fly ash in soil stabilization presents both advantages and disadvantages in engineering applications. One of the primary advantages lies in the economic viability of MSWI fly ash as a by-product, providing a cost-effective alternative for soil treatment. Its application offers a sustainable and eco-friendly solution, utilizing a waste material that would otherwise contribute to landfill.

Additionally, the research conducted by the authors contributes valuable insights into alternative soil solidification methods, expanding the range of available options for engineering applications. However, it is crucial to acknowledge the potential disadvantages associated with MSWI fly ash. The presence of heavy metals in the fly ash, such as Ni, Cd, Pb, As, and Hg, raises environmental concerns, necessitating careful monitoring and adherence to regulatory standards to prevent soil and water contamination. Variability in the composition of MSWI fly ash from different sources may pose challenges in ensuring consistent performance, and the lack of well-established guidelines and standards for its application in soil stabilization may require careful consideration during engineering design. Balancing the economic advantages with environmental and application-specific considerations is essential for making informed decisions about the use of MSWI fly ash in soil stabilization projects.

**Acknowledgements** This research work is part of a research project (Project No IH18.01.5) sponsored by the SPARC Hub in the Department of Civil Engineering, Monash University, funded by the Australian Research Council (ARC) Industrial Transformation Research Hub (ITRH) Scheme (Project ID: IH180100010). The authors gratefully acknowledge the financial and in-kind support of RMIT University and Monash University. Also, the authors acknowledge the facilities, and the scientific and technical assistance of the RMIT University's Microscopy & Microanalysis Facility, a linked laboratory of the Microscopy Australia.

**Author contributions** Z. Zimar: Conceptualization, Experimental investigation, Writing—original draft D. Robert: Conceptualization, Resources, Writing—review & editing, Supervision, F. Giustozzi—Writing—review & editing, A. Zhou: Writing—review & editing, S. Setunge: Funding acquisition, and J. Kodikara: Funding acquisition.

**Funding** Open Access funding enabled and organized by CAUL and its Member Institutions.

## Declarations

**Conflict of interest** The authors declare that they have no known competing financial interests or personal relationships that could have appeared to influence the work reported in this paper.

**Open Access** This article is licensed under a Creative Commons Attribution 4.0 International License, which permits use, sharing, adaptation, distribution and reproduction in any medium or format, as long as you give appropriate credit to the original author(s) and the source, provide a link to the Creative Commons licence, and indicate if changes were made. The images or other third party material in this article are included in the article's Creative Commons licence, unless indicated otherwise in a credit line to the material. If material is not included in the article's Creative Commons licence and your intended use is not permitted by statutory regulation or exceeds the permitted use, you will need to obtain permission directly from the copyright holder. To view a copy of this licence, visit <http://creativecommons.org/licenses/by/4.0/>.

## References

1. A.u.s.t.r.a.l.i.a (2017) Standards, methods of testing soils for engineering purposes Soil compaction and density tests—determination of the dry density/moisture content relation of a soil using standard compactive effort, AS 1289.5.1.1:2017, SAI Global
2. A.u.s.t.r.a.l.i.a (2009) Standards, Methods of testing soils for engineering purposes Soil classification tests—Determination of the plastic limit of a soil—Standard method, AS 1289.3.2.1–2009, SAI Global
3. A.u.s.t.r.a.l.i.a. (2014) Standards, Methods of testing soils for engineering purposes Soil strength and consolidation tests—determination of the California bearing ratio of a soil—standard laboratory method for a remoulded specimen, AS 1289.6.1.1:2014, SAI Global
4. AASHTO (2017) Standard method of test for determining the resilient modulus of soils and aggregate materials, T307–99, American Association of State Highway and Transportation Officials, Washington, D.C. 20001
5. AASHTO (1993) AASHTO guide for design of pavement structures, Washington, D.C
6. Allam MM, Sridharan A (1981) Effect of wetting and drying on shear strength. *J Soil Mech Found Div* 107(4):421–438
7. Al-Mukhtar M, Khattab S, Alcover JF (2012) Microstructure and geotechnical properties of lime-treated expansive clayey soil. *Eng Geol* 139:17–27
8. ASTM (2015) Standard test methods for wetting and drying compacted soil-cement mixtures, ASTM D559/D559M-15, ASTM international, West Conshohocken, United States
9. Atkins M, Glasser F, Jack J (1995) Zeolite P in cements: its potential for immobilizing toxic and radioactive waste species. *Waste Manag* 15(2):127–135
10. A. Standards (2019) Part 3: Preparation of leachates—Bottle leaching procedure
11. Australia S (2008) Methods for preparation and testing of stabilized materials Unconfined compressive strength of compacted materials, AS 5101.4–2008, SAI Global
12. Austroads G (2012) to pavement technology, part 2: pavement structural design. Australia, Sydney
13. Austroads (2019) Guide to pavement technology part 4D: stabilised materials. Austroads, Sydney NSW 2000 Australia
14. Bell F (1996) Lime stabilization of clay minerals and soils. *Eng Geol* 42(4):223–237
15. Bhatt A, Priyadarshini S, Mohanakrishnan AA, Abri A, Sattler M, Techapaphawit S (2019) Physical, chemical, and geotechnical properties of coal fly ash: a global review. *Case Stud Constr Mater* 11:e00263
16. Bhuvaneshwari S, Robinson R, Gandhi S (2019) Resilient modulus of lime treated expansive soil. *Geotech Geol Eng* 37:305–315
17. Blissett R, Rowson N (2012) A review of the multi-component utilisation of coal fly ash. *Fuel* 97:1–23
18. Brooks R, Udoyo FF, Takkalapelli KV (2011) Geotechnical properties of problem soils stabilized with fly ash and limestone dust in Philadelphia. *J Mater Civ Eng* 23(5):711–716
19. Caccamo MT, Mavilia G, Mavilia L, Lombardo D, Magazù S (2020) Self-assembly processes in hydrated montmorillonite by FTIR investigations. *Materials* 13(5):1100
20. Chen FH (2012) Foundations on expansive soils. Elsevier
21. Chen R, Congress SSC, Cai G, Zhou R, Xu J, Duan W, Liu S (2023) Evaluating the effect of active ions on the early performance of soft clay solidified by modified biomass waste-rice husk ash. *Acta Geotech* 18(2):1039–1056
22. Chen Z, Li J-S, Zhan B-J, Sharma U, Poon CS (2018) Compressive strength and microstructural properties of dry-mixed geopolymer pastes synthesized from GGBS and sewage sludge ash. *Constr Build Mater* 182:597–607
23. Cheng Q, Tang CS, Xu D, Zeng H, Shi B (2021) Water infiltration in a cracked soil considering effect of drying-wetting cycles. *J Hydrol* 593:125640
24. Chittoori B, Puppala AJ, Pedarla A (2018) Addressing clay mineralogy effects on performance of chemically stabilized expansive soils subjected to seasonal wetting and drying. *J Geotech Geoenviron Eng* 144:04017097
25. Cokca E (2001) Use of class C fly ashes for the stabilization of an expansive soil. *J Geotech Geoenviron Eng* 127(7):568–573
26. Consoli NC, Tonini de Araújo M, Tonatto Ferrazzo S, de Lima Rodrigues V, Gravinada Rocha C (2021) Increasing density and cement content in stabilization of expansive soils: Conflicting or complementary procedures for reducing swelling? *Can Geotech J* 58(6):866–878
27. Derrick MR, Stulik D, Landry JM (2000) Infrared spectroscopy in conservation science. Getty Publications, Los Angeles
28. de Brito Galvão TC, Elsharief A, Simões GF (2004) Effects of lime on permeability and compressibility of two tropical residual soils. *J Environ Eng* 130(8):881–885
29. D.o.W.a.E.R. Western Australia (2019) Landfill waste classification and waste definitions 1996 (as amended 2019), Department of Water and Environmental Regulation, Western Australia
30. Du YJ, Wu J, Bo YL, Jiang NJ (2020) Effects of acid rain on physical, mechanical and chemical properties of GGBS–MgO-solidified/stabilized Pb-contaminated clayey soil. *Acta Geotech* 15:923–932
31. Edil TB, Acosta HA, Benson CH (2006) Stabilizing soft fine-grained soils with fly ash. *J Mater Civ Eng* 18(2):283–294
32. E.P.A. Adelaide (2010) Current criteria for the classification of waste—including Industrial and Commercial Waste (Listed) and Waste Soil, Adelaide SA 5001
33. E.P.A. NSW (2014) Waste classification guidelines part 1: classifying waste, NSW EPA (Environment Protection Authority)
34. E.P.A. Tasmania (2018) Classification and management of contaminated soil for disposal Tasmania, Australia
35. E.P.A. Victoria (2021) Waste disposal categories—characteristics and thresholds, Victoria, Australia
36. Fasihnikoutalab MH, Pourakbar S, Ball RJ, Unluer C, Cristelo N (2020) Sustainable soil stabilisation with ground granulated blast-furnace slag activated by olivine and sodium hydroxide. *Acta Geotech* 15:1981–1991
37. Ferguson G, Levorson SM (1999) Soil and pavement base stabilization with self-cementing coal fly ash, American Coal Ash Association, Alexandria, VA
38. Fredlund D, Bergan A, Wong P (1977) Relation between resilient modulus and stress conditions for cohesive subgrade soils. *J Transp Res Rec* (642)
39. Fuoco R, Ceccarini A, Tassone P, Wei Y, Brongo A, Francesconi S (2005) Innovative stabilization/solidification processes of fly ash from an incinerator plant of urban solid waste. *Microchem J* 79(1–2):29–35
40. Galiano YL, Pereira CF, Vale J (2011) Stabilization/solidification of a municipal solid waste incineration residue using fly ash-based geopolymers. *J Hazard Mater* 185(1):373–381
41. Gevaudan JP, Campbell KM, Kane TJ, Shoemaker RK, Srubar WV III (2017) Mineralization dynamics of metakaolin-based alkali-activated cements. *Cem Concr Res* 94:1–12
42. Ghobadi M, Abdilor Y, Babazadeh R (2014) Stabilization of clay soils using lime and effect of pH variations on shear strength parameters. *Bull Eng Geol Environ* 73(2):611–619

43. Ghosh A, Subbarao C (1998) Hydraulic conductivity and leachate characteristics of stabilized fly ash. *J Environ Eng* 124(9):812–820
44. Gross AW (2020) *Cement-Stabilized Subgrade Soils*, Iowa State University, Washington, DC 20001
45. He Y, Cui YJ, Ye WM, Conil N (2017) Effects of wetting-drying cycles on the air permeability of compacted Téguline clay. *Eng Geol* 228:173–179
46. Hoang T, Do H, Alleman J, Cetin B, Dayioglu AY (2023) Comparative evaluation of freeze and thaw effect on strength of BEICP-stabilized silty sands and cement-and fly ash-stabilized soils. *Acta Geotech* 18(2):1073–1092
47. Hoornweg D, Bhada-Tata P (2012) What a waste: a global review of solid waste management
48. Hu Y, Vu HQ, Hubble DW (2010) Evaluation of dielectric-based probes for expansive soils: application to Regina clay. *Can Geotech J* 47(3):346–358
49. IOWA (2022) *Statewide Urban Design and Specifications Program (SUDAS) Design Manual*, Ames, IA, United States
50. Irshidat MR, Al-Nuaimi N, Rabie M (2021) Potential utilization of municipal solid waste incineration ashes as sand replacement for developing sustainable cementitious binder. *Constr Build Mater* 312:125488
51. Jameson G (2019) *Guide to pavement technology part 4D: stabilised materials*
52. Janz M, Johansson S-E (2002) The function of different binding agents in deep stabilization. *Swed Deep Stabil Res Centre Rep* 9:1–35
53. Jayakody S, Hemal G, Wijerathna H, Zimar A (2019) Particle breakage potential of recycled construction and demolition waste (RCDW) as an unbound pavement material. In: 9th International conference on sustainable built environment
54. Jayakody S, Zimar A, Ranaweera R (2018) Potential use of recycled construction and demolition waste aggregates for non-structural concrete applications
55. Jones LD, Jefferson I (2012) *Expansive soils*
56. Jose A, Nivitha M, Krishnan JM, Robinson R (2020) Characterization of cement stabilized pond ash using FTIR spectroscopy. *Constr Build Mater* 263:120136
57. Kamon M, Katsumi T, Sano Y (2000) MSW fly ash stabilized with coal ash for geotechnical application. *J Hazard Mater* 76(2–3):265–283
58. Kang X, Kang GC, Chang KT, Ge L (2015) Chemically stabilized soft clays for road-base construction. *J Mater Civ Eng* 27(7):04014199
59. Kavak A, Baykal G (2012) Long-term behavior of lime-stabilized kaolinite clay. *Environ Earth Sci* 66:1943–1955
60. Kayabali K, Demir S (2011) Measurement of swelling pressure: direct method versus indirect methods. *Can Geotech J* 48(3):354–364
61. Khattab S, Al-Mukhtar M, Fleureau J (2007) Long-term stability characteristics of a lime-treated plastic soil. *J Mater Civ Eng* 19(4):358–366
62. Ma W, Hoffmann G, Schirmer M, Chen G, Rotter VS (2010) Chlorine characterization and thermal behavior in MSW and RDF. *J Hazard Mater* 178(1–3):489–498
63. Mamatha K, Dinesh S (2017) Resilient modulus of black cotton soil. *Int J Pav Res Technol* 10(2):171–184
64. Marc JR (2022) The current worldwide WTE trend, 2019. <https://www.mswmanagement.com/collection/article/13036128/the-current-worldwide-wte-trend>. (Accessed 10.01.2022 2022)
65. Mir B, Sridharan AJG (2013) Physical and compaction behaviour of clay soil-fly ash mixtures. *Geotech Geol Eng* 31(4):1059–1072
66. Nalbantoglu Z (2004) Effectiveness of class C fly ash as an expansive soil stabilizer. *Constr Build Mater* 18(6):377–381
67. Nasrizar A-M, Muttharam M (2019) Effect of lime treatment on California bearing ratio (CBR) of expansive soils. *Int J Innov Sci Res Technol* 4(6):287–293
68. Nowak B, Pessl A, Aschenbrenner P, Szentannai P, Mattenberger H, Rechberger H, Hermann L, Winter F (2010) Heavy metal removal from municipal solid waste fly ash by chlorination and thermal treatment. *J Hazard Mater* 179(1–3):323–331
69. Odadjima H, Noto S, Nishikawa J, Yamazaki T (1995) Cement stabilization of peaty ground with consideration of organic matter. In: *Proceedings of international workshop on engineering characteristics and behavior of peat*
70. Okoronkwo MU, Mondal SK, Wang B, Ma H, Kumar A (2021) Formation and stability of gismondine-type zeolite in cementitious systems. *J Am Ceram Soc* 104(3):1513–1525
71. Pandian N, Krishna K, Sridharan A (2001) California bearing ratio behavior of soil/fly ash mixtures. *J Test Eval* 29(2):220–226
72. Pinilla JD, Miller GA, Cerato AB, Sneath DS (2011) Influence of curing time on the resilient modulus of chemically stabilized soils. *Geotech Test J* 34(4):364–372
73. Plank J, Winter C (2008) Competitive adsorption between superplasticizer and retarder molecules on mineral binder surface. *Cem Concr Res* 38(5):599–605
74. Pooni J, Robert D, Giustozzi F, Setunge S, Xie Y, Xia J (2020) Novel use of calcium sulfoaluminate (CSA) cement for treating problematic soils. *Constr Build Mater* 260:120433
75. Poran CJ, Ahtchi-Ali F (1989) Properties of solid waste incinerator fly ash. *J Geotech Eng* 115(8):1118–1133
76. Prusinski JR, Bhattacharja S (1999) Effectiveness of Portland cement and lime in stabilizing clay soils. *Transp Res Rec* 1652(1):215–227
77. Puppala AJ, Ramakrishna AM, Hoyos LR (2003) Resilient moduli of treated clays from repeated load triaxial test. *Transp Res Rec* 1821(1):68–74
78. Quina MJ, Bordado JC, Quinta-Ferreira RM (2008) Treatment and use of air pollution control residues from MSW incineration: an overview. *Waste Manag* 28(11):2097–2121
79. Rahman MA, Imteaz MA, Arulrajah A, Piratheepan J, Disfani MM (2015) Recycled construction and demolition materials in permeable pavement systems: geotechnical and hydraulic characteristics. *J Clean Prod* 90:183–194
80. Rayment GE, Lyons DJ (2011) *Soil chemical methods: Australasia*, CSIRO publishing
81. Renjith R, Robert D, Setunge S, Costa S, Mohajerani A (2021) Optimization of fly ash based soil stabilization using secondary admixtures for sustainable road construction. *J Clean Prod* 294:126264
82. Saja AMA, Zimar AMZ, Junaideen SM (2021) Municipal solid waste management practices and challenges in the southeastern coastal cities of Sri Lanka. *Sustainability* 13(8):4556
83. Senol A, Edil TB, Bin-Shafique MS, Acosta HA, Benson CH (2006) Soft subgrades' stabilization by using various fly ashes. *Resour Conserv Recycl* 46(4):365–376
84. Shahack-Gross R, Bar-Yosef O, Weiner S (1997) Black-coloured bones in Hayonim Cave, Israel: differentiating between burning and oxide staining. *J Archaeol Sci* 24(5):439–446
85. Sorell G (1997) The role of chlorine in high temperature corrosion in waste-to-energy plants. *Mater High Temp* 14(3):207–220
86. Sperinck S, Raiteri P, Marks N, Wright K (2011) Dehydroxylation of kaolinite to metakaolin—a molecular dynamics study. *J Mater Chem* 21(7):2118–2125
87. Tang Q, Zhang Y, Gao Y, Gu F (2017) Use of cement-chelated, solidified, municipal solid waste incinerator (MSWI) fly ash for pavement material: mechanical and environmental evaluations. *Can Geotech J* 54(11):1553–1566

88. Toussaint F, Fripiat J, Gastuche M (1963) Dehydroxylation of kaolinite. I. Kinetics. *J Phys Chem* 67(1):26–30
89. Turan C, Javadi AA, Vinai R (2022) Effects of class C and class F fly ash on mechanical and microstructural behavior of clay soil—a comparative study. *Materials* 15(5):1845
90. Vieira GL, Schiavon JZ, Borges PM, da Silva SR, de Oliveira Andrade JJ (2020) Influence of recycled aggregate replacement and fly ash content in performance of pervious concrete mixtures. *J Clean Prod* 271:122665
91. Vizcarra GOC, Casagrande M, da Motta LM (2014) Applicability of municipal solid waste incineration ash on base layers of pavements. *J Mater Civ Eng* 26(6):06014005
92. Wang X, Zhang Z, Song Z, Li J (2022) Engineering properties of marine soft clay stabilized by alkali residue and steel slag: an experimental study and ANN model. *Acta Geotech* 17(11):5089–5112
93. Wiles C, Shepherd P (1999) Beneficial use and recycling of municipal waste combustion residues—a comprehensive resource document. National Renewable Energy Lab., Golden, CO (US)
94. Xia WY, Du YJ, Li FS, Li CP, Yan XL, Arulrajah A, Wang F, Song DJ (2019) In-situ solidification/stabilization of heavy metals contaminated site soil using a dry jet mixing method and new hydroxyapatite based binder. *J Hazard Mater* 369:353–361
95. Ylmén R, Jäglid U, Steenari B-M, Panas I (2009) Early hydration and setting of Portland cement monitored by IR SEM and Vicat techniques. *Cem Concr Res* 39(5):433–439
96. Yoobanpot N, Jamsawang P, Poorahong H, Jongpradist P, Likitlersuang S (2020) Multiscale laboratory investigation of the mechanical and microstructural properties of dredged sediments stabilized with cement and fly ash. *Eng Geol* 267:105491
97. Youcai Z, Lijie S, Guojian L (2002) Chemical stabilization of MSW incinerator fly ashes. *J Hazard Mater* 95(1–2):47–63
98. Zha F, Liu S, Du Y, Cui K (2008) Behavior of expansive soils stabilized with fly ash. *Nat Hazards* 47(3):509–523
99. Zhang S, Ghouleh Z, He Z, Hu L, Shao Y (2021) Use of municipal solid waste incineration bottom ash as a supplementary cementitious material in dry-cast concrete. *Constr Build Mater* 266:120890
100. Zimar Z, Robert D, Sidiq A, Zhou A, Giustozzi F, Setunge S, Kodikara J (2022) Waste-to-energy ash for treating highly expansive clays in road pavements. *J Clean Prod* 374:133854
101. Zimar Z, Robert D, Zhou A, Giustozzi F, Setunge S, Kodikara J (2022) Application of coal fly ash in pavement subgrade stabilisation: a review. *J Environ Manag* 312:114

**Publisher's Note** Springer Nature remains neutral with regard to jurisdictional claims in published maps and institutional affiliations.